

Dynamical Conductivity of Disordered Quantum Hall Stripes

Mei-Rong Li¹, H.A. Fertig^{2,3}, R. Côté¹, Hangmo Yi⁴

¹*Département de Physique, Université de Sherbrooke, Sherbrooke, Québec, Canada J1K 2R1*

²*Department of Physics and Astronomy, University of Kentucky, Lexington, Kentucky 40506-0055*

³*Department of Physics, Indiana University, Bloomington, IN 47405*

⁴*Department of Physics, Soongsil University, Seoul, 156-743, Korea*

(Dated: November 1, 2018)

We present a detailed theory for finite-frequency conductivities $\text{Re}[\sigma_{\alpha\beta}(\omega)]$ of quantum Hall stripes, which form at Landau level $N \geq 2$ close to half filling, in the presence of weak Gaussian disorder. We use an effective elastic theory to describe the low-energy dynamics of the stripes with the dynamical matrix being determined through matching the density-density correlation function obtained in the microscopic time-dependent Hartree-Fock approximation. We then apply replicas and the Gaussian variational method to deal with the disorder. Within this method, a set of saddle point equations for the retarded self energies are obtained, which are solved numerically to get $\text{Re}[\sigma_{\alpha\beta}(\omega)]$. We find a quantum depinning transition as $\Delta\nu$, the fractional part of the filling factor, approaches a critical value $\Delta\nu_c$ from below. For $\Delta\nu < \Delta\nu_c$, the pinned state is realized in a replica symmetry breaking (RSB) solution, and the frequency-dependent conductivities in both the directions perpendicular and parallel to the stripes show resonant peaks. These peaks shift to zero frequency as $\Delta\nu \rightarrow \Delta\nu_c$. For $\Delta\nu \geq \Delta\nu_c$, we find a *partial RSB (PRSB)* solution in which there is RSB perpendicular to the stripes, but replica symmetry along the stripes, leading to free sliding along the stripe direction. The quantum depinning transition is in the Kosterlitz-Thouless universality class. The result is consistent with a previous renormalization group analysis.

PACS numbers: 73.43.Nq, 73.43.Lp, 73.43.Qt

I. INTRODUCTION

Charge density waves (CDWs) may form in many correlated electronic systems when the Coulomb interaction dominates over the kinetic energy. For a two-dimensional electron gas in a perpendicular magnetic field, the quantization of the kinetic energy into Landau levels can enhance this possibility¹. Each Landau level is highly degenerate, with the number of states equal to the number of magnetic flux quanta passing through the system. If the field and corresponding degeneracy is sufficiently large, the low-energy physics of the system may then be dominated by electrons in the highest partially occupied (N th) Landau level, with the other electrons essentially renormalizing the effective Coulomb interaction in this level². In this situation, the kinetic energy is quenched and the system arranges itself in order to minimize the interactions. The Hartree-Fock approximation¹ predicts the formation of CDW ground states for $N \geq 2$. These CDWs evolve from Wigner crystals to “bubble states”¹ as the partial Landau-level filling factor $\Delta\nu$ increases. For $\Delta\nu \gtrsim 0.4$, the bubble states give way to stripe states (also called unidirectional CDWs.) This Hartree-Fock result is corroborated by density matrix renormalization group calculations³ and exact diagonalization studies⁴. DC transport experiments indeed observe highly anisotropic, and apparently metallic, conductivity⁵ near half-filling of higher Landau levels ($N \geq 2$). This is likely due to the formation of stripe states.

Because the stripe state breaks translational symmetry in only one direction, it has the symmetry of a smectic liquid crystal⁶, and as in that system supports a set of gapless phonon modes⁷. These modes are present because the stripe state lacks any restoring force when a single stripe slides with respect to the others. In the context of an electron system, the smectic state can be thought of as a self-organized array of Luttinger liquids^{6,8}, a state of fermions that does not obey Landau Fermi liquid theory and (so far) is known to exist only in one dimension⁹. One way of viewing the Luttinger liquid is in terms of a one dimensional crystal that has lost long-range order due to quantum fluctuations¹⁰. This idea is easily generalized to the case of stripes¹¹, and suggests that the low-energy degrees of freedom for the system may be described in terms of a displacement field. This will be the basic language for our study.

It has long been recognized that disorder can pin a CDW and render it insulating^{12,13}. (Similarly, Luttinger liquids may be pinned by impurities in spite of their liquid-like correlations¹⁴.) In this situation, the real part of the zero wavevector, finite-frequency conductivity $\sigma_{\alpha\beta}(\omega)$ vanishes as $\omega \rightarrow 0$, and has a resonance at higher ω with a peak (or pinning) frequency and width that are determined by the effective restoring force due to the disorder¹². Such behavior has indeed been observed in high Landau levels for $\Delta\nu$ sufficiently far away from 1/2 so that one expects the electrons to be organized into bubble states¹⁵. As $\Delta\nu$ is increased, there is a general trend for the pinning frequency to decrease, eventually becoming lost in the noise as the filling factor approaches the value at which the DC conductivity becomes anisotropic and metallic⁵. Experiments to better resolve the dynamical conductivity as the stripe phase is entered are currently underway¹⁶.

A fundamental question that arises in this context is whether the apparent metallic behavior seen in DC transport experiments represents the true zero temperature behavior in the stripe state. While current data suggests the diagonal conductivities σ_{xx} and σ_{yy} saturate to finite values at low temperatures, presumably such experiments can answer this fundamental question unambiguously only by reaching significantly lower temperatures than are currently available. The possibility that near half-filling the stripes may not be fully pinned is extremely intriguing because, if this is indeed the case, then the electrons have avoided becoming localized and the resulting anisotropic metal cannot be a Fermi liquid. Thus this state could well be a higher dimensional analogue of a Luttinger liquid. Developing and understanding the results of experiments beyond DC transport – such as measurements of the dynamical conductivity¹⁵ – then take on an additional significance.

One possible route to metallic behavior for the stripe system could be via a depinning transition. In principle this could happen in a one dimensional Luttinger liquid, if one could continuously tune the interactions from repulsive to attractive¹⁴. Because the stripe system has a larger parameter space needed to describe its elastic properties than the single stiffness that describes a one-dimensional solid (specifically, one needs to estimate the dynamical matrix along a line in the Brillouin zone, as we discuss below), it is possible to arrive at this depinning transition even when the bare interaction parameters among the electrons are purely repulsive¹¹. The question of whether stripes may become depinned must be answered via a detailed calculation of the stripe elasticity, and depending on how one estimates this, different answers are possible^{8,17}, as we discuss in more detail below.

In what follows, we will adopt an approach that models the quantum Hall (QH) stripe system as an array of one dimensional, quantum disordered solids as shown in Fig. 1. We estimate the dynamical matrix of this system by matching the elastic theory to the results of a microscopic calculation within the time-dependent Hartree-Fock approximation (TDHFA). This approach was taken by some of us¹⁷ in a perturbative renormalization group (RG) calculation, which demonstrated that a quantum depinning transition can occur as $\Delta\nu \rightarrow \Delta\nu_c$ from below, with the critical partial filling $\Delta\nu_c$ depending on the details of the system: Landau level index, layer thickness, disorder strength, etc. Our goal is to compute the dynamical conductivity as the system passes through the transition, to identify signatures that would indicate that the system has passed into an unpinned stripe state. A brief summary of our major results has been published elsewhere¹⁸. In this article, we provide details of the calculations as well as some further results.

Our general approach to this problem is to use replicas¹⁹ and the Gaussian variational method (GVM), as was first introduced by Mézard and Parisi for elastic manifolds²⁰ and then further developed by Giamarchi and Le Doussal and their coworkers in applications to a variety of condensed matter systems^{21–24}. In the QH systems, this method was used by Chitra *et al.*²⁴ for pinned Wigner crystals in the $N = 0$ Landau level, and by Orignac and Chitra²⁵ for stripes, in the latter case using a different set of approximations than us and yielding very different results than those described below. Because of the strong fluctuations inherent in the depinning transition, we have found that one cannot correctly solve for the dynamical conductivity using the “semiclassical approximation” to the saddle point equations (SPE’s), which we review below, that has given this approach its attractive simplicity. By relaxing this approximation we will see that in the depinned state the dynamical conductivity can have a surprising power-law frequency dependence, and a discontinuous behavior at the transition that is analogous to the universal stiffness jump that occurs at a Kosterlitz-Thouless (KT) transition²⁶. Moreover, we will see that the solution to the SPE’s that yield this behavior have an unusual structure involving breaking the replica symmetry for motion perpendicular to the stripes, while preserving it parallel to the stripes. This *partial replica symmetry breaking* (PRSB) indicates that the stripes may be pinned for perpendicular motion while free to slide relative to one another. This qualitative behavior was anticipated by the perturbative RG study¹⁷.

As discussed above, when the system is pinned there are resonant peaks which appear in σ_{xx} and σ_{yy} . (We choose the \hat{x} direction to be perpendicular to the stripes, and the \hat{y} direction to be parallel to it as shown in Fig. 1. Of course, the two diagonal conductivities are not the same due to the anisotropy of the stripe state.) The peaks drop to zero frequency as $\Delta\nu_c$ is approached from below, with their weights increasing for motion along the stripes, and decreasing for motion perpendicular to them. As the transition is approached, the resonance peaks become increasingly asymmetric. Upon crossing the transition, σ_{yy} develops a δ -function at $\omega = 0$, indicating superconducting behavior, while σ_{xx} rises from zero as a power of ω . This unusual behavior is a result of the power-law correlations associated with the Luttinger liquid-like behavior of the unpinned state. We note that our $\omega = 0$ results are not consistent with the DC conductivity results seen in experiments, although preliminary experimental results for finite frequency do bear some resemblance to our predictions¹⁶. We will comment below on what is missing from our model that we believe leads to this discrepancy.

This paper is organized as follows. In Sec. II we review the procedure for determining the dynamical matrix in the elastic model. This is followed by a review in Sec. III of the qualitative effects of disorder within the RG analysis. In Sec. IV, we review the replica and GVM which leads to a set of saddle point equations (SPE’s) for the self energy. Solutions of the SPE’s and the result for the conductivities are presented in Sec. V, focusing on the pinned state for $\Delta\nu < \Delta\nu_c$, and in Sec. VI, which is devoted to the depinned state for $\Delta\nu > \Delta\nu_c$. We discuss the nature of the depinning transition in Sec. VII, and conclude in Sec. VIII. There are four appendices: the first summarizes the

Hartree-Fock (HF) and the TDHFA formalisms, the result of which is used for determination of the dynamical matrix; the second gives a derivation for the inversion rules needed for hierarchical matrices of the type dealt with in this paper; the third discusses analytic continuation of the dynamical conductivity from imaginary time to real time; and the fourth discusses another possible solution to the SPE's that has unphysical properties.

II. ELASTIC MODEL OF QH STRIPES

A. Elastic action

In our approach, low energy distortions from the mean-field state are described by an elastic model, with displacement fields $u_x(\mathbf{r})$ and $u_y(\mathbf{r})$ representing the effective dynamical variables of the QH stripes. Fig. 1 shows schematically the one-dimensional arrays modelling the stripes. They obey single Landau level dynamics²⁷ $[u_x(\mathbf{R}), u_y(\mathbf{R}')] = il_B^2 \delta_{\mathbf{R}, \mathbf{R}'}$, where $l_B = \sqrt{\hbar c/eB}$ is the magnetic length. In the pure limit, the Euclidean action of the elastic model may be written as (throughout this work, we use the unit $k_B = \hbar = 1$)

$$S_0 = \frac{1}{2T} \sum_{\mathbf{q}, \omega_n} \sum_{\alpha, \beta=x, y} u_\alpha(\mathbf{q}, \omega_n) G_{\alpha\beta}^{(0)-1}(\mathbf{q}, \omega_n) u_\beta(-\mathbf{q}, -\omega_n), \quad (1)$$

where T is the temperature, $\omega_n (= 2\pi n/T)$ the bosonic Matsubara frequency, and

$$G_{\alpha\beta}^{(0)}(\mathbf{q}, i\omega_n) = \frac{l_B^4}{(\omega_n^2 + \omega_{\mathbf{q}}^2)} \begin{pmatrix} D_{yy}(\mathbf{q}) & \frac{\omega_n}{l_B^2} - D_{xy}(\mathbf{q}) \\ -\frac{\omega_n}{l_B^2} - D_{yx}(\mathbf{q}) & D_{xx}(\mathbf{q}) \end{pmatrix}_{\alpha\beta} \quad (2)$$

is the unperturbed Green's function of the displacement fields with $D_{\alpha\beta}(\mathbf{q})$ being the dynamical matrix and

$$\omega_{\mathbf{q}} = l_B^2 \sqrt{D_{xx}(\mathbf{q}) D_{yy}(\mathbf{q}) - D_{xy}^2(\mathbf{q})} \quad (3)$$

being a general expression for phonon modes of a charged elastic system in a strong magnetic field (magnetophonon modes). As always for a Gaussian theory, the correlation function may be expressed in terms of the Green's function via

$$G_{\alpha\beta}^{(0)}(\mathbf{q}, \omega_n) = \int_0^{1/T} d\tau e^{i\omega_n \tau} \langle \mathcal{T}_\tau u_\alpha(\mathbf{q}, \tau) u_\beta(-\mathbf{q}, 0) \rangle_{S_0}, \quad (4)$$

where $\langle \dots \rangle_{S_0}$ denotes an average over the displacement fields with the usual weighting factor e^{-S_0} , and \mathcal{T}_τ is the imaginary time ordering operator.

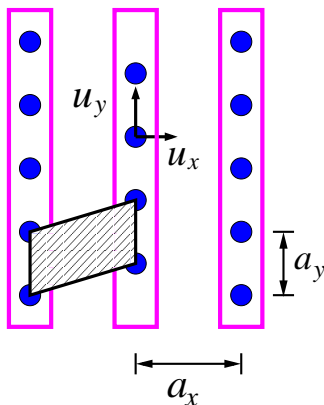


FIG. 1: Schematic diagram of quasi one-dimensional arrays modelling the QH stripes. The stripes are along the \hat{y} direction, and u_x and u_y are the displacement fields. The shaded area is the unit cell of the stripes crystal with the volume $a_x a_y$.

Because of inversion and reflection symmetries, and the fact that the dynamical matrix elements in real space are real, we have

$$D_{\alpha\beta}(\mathbf{q}) = D_{\beta\alpha}(-\mathbf{q}), \quad (5)$$

$$D_{xy}(\mathbf{q}) = D_{yx}(\mathbf{q}), \quad (6)$$

$$D_{xy}(q_x, q_y) = -D_{xy}(-q_x, q_y) = -D_{xy}(q_x, -q_y), \quad (7)$$

so that the unperturbed Green's function has the symmetries

$$G_{\alpha\alpha}^{(0)}(\mathbf{q}, \omega_n) = G_{\alpha\alpha}^{(0)}(-\mathbf{q}, \omega_n) = G_{\alpha\alpha}^{(0)}(\mathbf{q}, -\omega_n) = G_{\alpha\alpha}^{(0)}(-\mathbf{q}, -\omega_n), \quad (8)$$

$$G_{xy}^{(0)}(\mathbf{q}, \omega_n) = G_{yx}^{(0)}(\mathbf{q}, -\omega_n), \quad (9)$$

$$G_{xy}^{(0)}(q_x, q_y, \omega_n) = G_{xy}^{(0)}(-q_x, -q_y, \omega_n) = -G_{xy}^{(0)}(-q_x, q_y, \omega_n) = -G_{xy}^{(0)}(q_x, -q_y, \omega_n). \quad (10)$$

To perform quantitative calculations, it is necessary to produce estimates of the dynamical matrix elements $D_{\alpha\beta}(\mathbf{q})$ for the QH stripe states. We do this with a matching procedure that uses results from microscopic TDHFA computations. Below we briefly review this matching procedure.

B. Relation between $G_{\alpha\beta}^{(0)}(\mathbf{q}, \omega)$ and guiding-center density-density correlation function

In a classical model, each site of the crystal is occupied by an electron whose charge density is specified by a form factor $f(\mathbf{r})$ (with $\int d\mathbf{r} f(\mathbf{r}) = 1$). In the absence of any fluctuations these electrons will lie on the oblique Bravais lattice as shown in Fig. 1. Fluctuations around this reference state are given in terms of the displacement fields $\mathbf{u}(\mathbf{R})$. The time-dependent electronic density is then written as

$$n(\mathbf{r}, t) = \sum_{\mathbf{R}} f(\mathbf{r} - \mathbf{R} - \mathbf{u}(\mathbf{R}, t)). \quad (11)$$

The Fourier transform of this density is given by

$$n(\mathbf{q}, t) = \int d\mathbf{r} e^{-i\mathbf{q}\cdot\mathbf{r}} n(\mathbf{r}, t) \approx f(\mathbf{q})\delta_{\mathbf{q},\mathbf{K}} - if(\mathbf{q})\sqrt{N_s}\mathbf{q} \cdot \mathbf{u}(\mathbf{q}), \quad (12)$$

where N_s is the number of crystal sites or electrons and \mathbf{K} is a reciprocal lattice vector. The form factor $f(\mathbf{r})$ is real and has inversion symmetry so that $f(\mathbf{q})$ is real.

The fact that the density fluctuations are related to the displacement field via

$$\delta n(\mathbf{q} + \mathbf{K}, t) \approx -if(\mathbf{q} + \mathbf{K})\sqrt{N_s}(\mathbf{q} + \mathbf{K}) \cdot \mathbf{u}(\mathbf{q}) \quad (13)$$

(with \mathbf{q} a vector in the first Brillouin zone of the reciprocal lattice) implies that we can relate the displacement Green's function $G_{\alpha\beta}^{(0)}(\mathbf{q}, \omega)$ to the density-density correlation function $\chi_{\mathbf{K},\mathbf{K}'}^{(n,n)}(\mathbf{q}, \tau)$ (introduced in Appendix A) through

$$\chi_{\mathbf{K},\mathbf{K}'}^{(n,n)}(\mathbf{q}, \tau) = -N_s f(\mathbf{q} + \mathbf{K}) f(\mathbf{q} + \mathbf{K}') \left[(\mathbf{q} + \mathbf{K}) \cdot \widehat{G}^{(0)}(\mathbf{q}, \tau) \cdot (\mathbf{q} + \mathbf{K}') \right]. \quad (14)$$

Here $\chi_{\mathbf{K},\mathbf{K}'}^{(n,n)}(\mathbf{q}, \tau)$ is a quantity that we compute in the microscopic TDHFA⁷. In Appendix A, we summarize the HF and TDHF formalisms. Eq. (A14) there will be used for the determination of the dynamical matrix. Substituting Eq. (2) in Eq. (14) yields

$$\chi_{\mathbf{K},\mathbf{K}'}^{(n,n)}(\mathbf{q}, i\omega_n) = -\frac{N_s l_B^4}{(\omega_n^2 + \omega_{\mathbf{q}}^2)} \left[\Gamma_1 + \Gamma_2 \frac{\omega_n}{l_B^2} \right] f(\mathbf{q} + \mathbf{K}) f(\mathbf{q} + \mathbf{K}'), \quad (15)$$

with the definitions

$$\Gamma_1 = -(\mathbf{q} + \mathbf{K}) \times \overleftrightarrow{D}(\mathbf{q}) \times (\mathbf{q} + \mathbf{K}'), \quad (16)$$

and

$$\Gamma_2 = (\mathbf{q} + \mathbf{K}) \times (\mathbf{q} + \mathbf{K}'). \quad (17)$$

The two-dimensional vector product in the last two equations stands for $\mathbf{a} \times \mathbf{b} = a_x b_y - a_y b_x$.

The analytical continuation of $\chi_{\mathbf{K},\mathbf{K}'}^{(n,n)}(\mathbf{q}, i\omega_n)$ in Eq. (15) results in

$$\chi_{\mathbf{K},\mathbf{K}'}^{(n,n)}(\mathbf{q}, \omega) = -N_s l_B^4 \left[\frac{Z}{\omega + i\delta + \omega_{\mathbf{q}}} - \frac{Z^*}{\omega + i\delta - \omega_{\mathbf{q}}} \right] f(\mathbf{q} + \mathbf{K}) f(\mathbf{q} + \mathbf{K}'), \quad (18)$$

where

$$Z = \frac{\Gamma_1}{2\omega_{\mathbf{K}}} - i \frac{\Gamma_2}{2l_B^2}. \quad (19)$$

We can now request that Eq. (18) be equivalent to Eq. (A14) in Appendix A in order to obtain the dynamical matrix. This requires that

$$\Delta\nu l_B^4 Z^* f(\mathbf{q} + \mathbf{K}) f(\mathbf{q} + \mathbf{K}') = F(\mathbf{q} + \mathbf{K}) F(\mathbf{q} + \mathbf{K}') W_i(\mathbf{q} + \mathbf{K}, \mathbf{q} + \mathbf{K}'), \quad (20)$$

where $W_i(\mathbf{q} + \mathbf{K}, \mathbf{q} + \mathbf{K}')$ is the weight associated with the magnetophonon frequency ε_i in the TDHFA response and $\Delta\nu = N/N_\varphi$ is the filling factor of the partially filled level. The magnetophonon frequency ε_i is found, at small wavevector \mathbf{q} , by locating the eigenvalue ε_i of the matrix M defined in Eq. (A11) with the biggest weight $W_i(\mathbf{q} + \mathbf{K}, \mathbf{q} + \mathbf{K})$ in the *diagonal* response function $\chi_{\mathbf{K}, \mathbf{K}}^{(n, n)}(\mathbf{q}, \omega)$.

A careful examination shows that, because $\omega_{\mathbf{q}}$ is given by the determinant of the matrix \hat{D} , the quantity $\Gamma_1/2\omega_{\mathbf{q}}$ is unchanged if all the components of the dynamical matrix are multiplied by some constant. Eq. (20) is thus indeterminate. To avoid this, we replace $\omega_{\mathbf{q}}$ by ε_i in this equation. Our final equation is then

$$f(\mathbf{q} + \mathbf{K}) f(\mathbf{q} + \mathbf{K}') [l_B^2 \Gamma_1 + i\varepsilon_i \Gamma_2] = \frac{2\varepsilon_i}{\Delta\nu l_B^2} F(\mathbf{q} + \mathbf{K}) F(\mathbf{q} + \mathbf{K}') W_i(\mathbf{q} + \mathbf{K}, \mathbf{q} + \mathbf{K}'). \quad (21)$$

With this equation, we can determine the 3 components of the dynamical matrix as well as the form factors $f(\mathbf{q} + \mathbf{K})$.

C. Matching procedure

At this point, it is worthwhile remarking that, in the HFA, there is an extremely small energy difference (of order $10^{-6} e^2/\kappa l_B$) between the energies of the stripe crystals with in-phase and out-of-phase modulation on adjacent stripes. As a result, the magnetophonon dispersion in the TDHFA has a very small gap in the perpendicular direction. This interstripe locking energy is, however, not accessible within our numerical accuracy so that our calculated magnetophonon dispersion is that appropriate for a smectic. In particular, it contains a line of gapless modes for $q_x \neq 0, q_y = 0$. Because of this nodal line, we need to fit the dynamical matrix for small q_y i.e., for long wavelengths along the stripes, and for all values of q_x in the Brillouin zone. Indeed, these low-energy modes play a crucial role in determining the effects of both quantum and thermal fluctuations on the system.

We choose to solve Eq. (21) for the shortest three reciprocal lattice vectors: $\mathbf{K}, \mathbf{K}' = (0, 0), (0, \pm K_{y0})$ where $K_{y0} = 2\pi/a_y$ with a_y being the lattice constant along the stripes direction (see Fig. 1). For each \mathbf{q} , the TDHFA calculation provides ten independent numbers, nine in the 3×3 Hermitian matrix $W_i(\mathbf{q} + \mathbf{K}, \mathbf{q} + \mathbf{K}')$ and one in ε_i . We use six of them to determine D_{xx}, D_{xy}, D_{yy} , and the three real parameters $f(\mathbf{q} + \mathbf{K})$. The rest may be used to check the consistency of the numerical procedure. The final result¹⁷ indicates that the matching is very accurate.

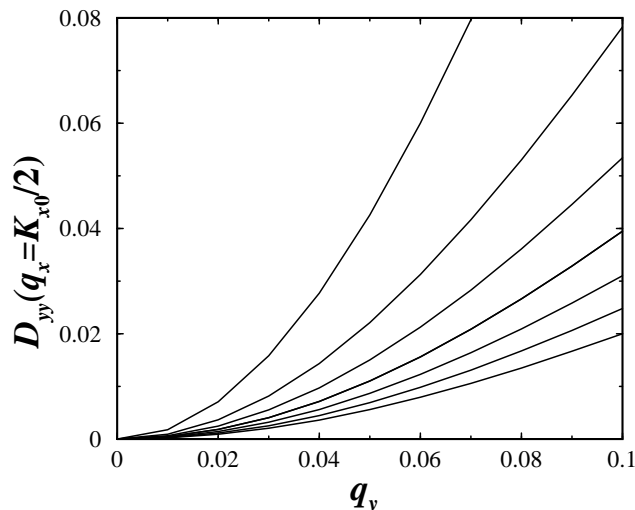


FIG. 2: Dynamical matrix D_{yy} as a function of q_y at small q_y and $q_x = K_{x0}/2$. Curves from right to left correspond to $\Delta\nu = 0.36, 0.38, 0.4, 0.42, 0.44, 0.46, 0.48$, respectively.

A typical result for $D_{yy}(\mathbf{q})$ as a function of q_y at small q_y and $q_x = K_{x0}/2$ is shown in Fig. 2. Clearly $D_{yy}(\mathbf{q})$ is quadratic in q_y . Indeed, based on symmetry considerations^{7,8}, the low energy sector of $\mathbf{D}(\mathbf{q})$ should have the form

for small q_y :

$$D_{xx}(\mathbf{q}) \simeq d_{xx}(q_x) + \kappa_b q_y^4, \quad (22)$$

$$D_{xy}(\mathbf{q}) \simeq d_{xy}(q_x) q_y, \quad (23)$$

$$D_{yy}(\mathbf{q}) \simeq d_{yy}(q_x) q_y^2, \quad (24)$$

where κ_b is the bending coefficient. The absence of a quadratic q_y term in D_{xx} follows from rotational symmetry and is the major difference between a smectic and a crystal dynamical matrix. In our calculation below, we will use this smectic form, determining $d_{xx}(q_x)$, $d_{xy}(q_x)$ and $d_{yy}(q_x)$ on a grid of q_x points numerically. The $\kappa_b q_y^4$ in Eq. (22) reflects the bending energy of the stripes. In practice, this term merely plays the role of high- q_y cutoff and thus κ_b is chosen for convenience to be 2 in our numerical calculation.

Inserting Eqs. (22-24) into Eq. (3) yields

$$\omega_{\mathbf{q}} \simeq l_B^2 \sqrt{d_{xx}(q_x) d_{yy}(q_x) - d_{xy}^2(q_x) q_y} \quad (25)$$

for small q_y .

Once the Green's function has been determined, we can easily compute the conductivity. Since the electric current is carried by the charge, the current density can be expressed as

$$\mathbf{j}(\mathbf{q}, \tau) = ie \frac{d\mathbf{u}(\mathbf{q}, \tau)}{d\tau}. \quad (26)$$

The conductivity is then determined by the Kubo formula to be

$$\sigma_{\alpha\beta}(\omega) = -\frac{1}{\omega a_x a_y} \left[\int_0^{1/T} d\tau e^{i\omega_n \tau} \langle j_\alpha(\mathbf{q}=0, \tau) j_\beta(\mathbf{q}=0, 0) \rangle \right]_{i\omega_n \rightarrow \omega + i0^+} = -\frac{e^2}{a_x a_y} i\omega G_{\alpha\beta}^{\text{ret}}(\mathbf{q}=0, \omega). \quad (27)$$

where a_x is the distance between the centers of two neighboring stripes (see Fig. 1). It is easy to check that in the pure limit, the electromagnetic response of the system is purely transverse. Calculating $G_{\alpha\beta}^{\text{ret}}$ in the presence of disorder is our next (and indeed most important) task.

III. QUALITATIVE EFFECT OF DISORDER

A. Modeling the disorder

We assume that the disorder can be modeled as a Gaussian random potential $V(\mathbf{r})$. The disorder action reads

$$S_{\text{imp}} = \int d\mathbf{r} \int_0^{1/T} d\tau V(\mathbf{r}) n(\mathbf{r}, \tau) \quad (28)$$

where $V(\mathbf{r})$ has the following Gaussian distribution function

$$P(V) = \exp \left[-\frac{1}{2} \int d\mathbf{r}_1 \int d\mathbf{r}_2 V(\mathbf{r}_1) \Gamma^{-1}(\mathbf{r}_1 - \mathbf{r}_2) V(\mathbf{r}_2) \right], \quad (29)$$

with

$$\Gamma(\mathbf{r}_1 - \mathbf{r}_2) = \overline{V(\mathbf{r}_1) V(\mathbf{r}_2)} = V_0^2 a_x a_y \delta(\mathbf{r} - \mathbf{r}'). \quad (30)$$

Here the overline denotes average over disorder:

$$\overline{A} = \frac{\int \mathcal{D}V P(V) A}{\int \mathcal{D}V P(V)}. \quad (31)$$

The electron density operator $n(\mathbf{r}, \tau)$ in Eq. (28) must, in order to capture the possibility of pinning by disorder, be approximated more accurately than was needed in the matching procedure discussed in the preceding section.

Following Giamarchi and Le Doussal²², under the assumption of small $\nabla\mathbf{u}(\mathbf{r})$ (which is justified for weak disorder) we write

$$n(\mathbf{q}, \tau) \simeq f(\mathbf{q}) \left[N_s - i\sqrt{N_s}\mathbf{q} \cdot \mathbf{u}(\mathbf{q}, \tau) + \sum_{\mathbf{K} \neq 0} \int d\mathbf{r} e^{i\mathbf{K} \cdot [\mathbf{r} - \mathbf{u}(\mathbf{r}, \tau)] - i\mathbf{q} \cdot \mathbf{r}} \right]. \quad (32)$$

This differs from our approximation in Eq. (12) essentially via the last term which captures the short wavelength oscillations in the charge density and allows pinning by impurities. In employing Eq. 32, since only the last term can actually lead to pinning²², we will drop the first two terms upon substitution into Eq. 28. Moreover, in the reciprocal lattice sum we retain only the smallest non-trivial wavevectors, so that in what follows (unless otherwise specified) $\sum_{\mathbf{K} \neq 0}$ really means sum over $\mathbf{K} = (\pm K_{x0}, 0), (0, \pm K_{y0}), (\pm K_{x0}, \pm K_{y0})$, where $K_{x0} = 2\pi/a_x$. These simplifications, we will see, allow us to compute the Green's function in a relatively straightforward manner while retaining the essential physics of pinning so that our results are qualitatively correct. The major effect of these approximations is to replace the soft cutoff in wavevector that would enter through the form factor with a hard one in the reciprocal lattice sum. With these approximations, the impurity action with which we work is

$$S'_{\text{imp}} = n_0 \int d\mathbf{r} d\tau V(\mathbf{r}) \sum_{\mathbf{K} \neq 0} e^{i\mathbf{K} \cdot [\mathbf{r} - \mathbf{u}(\mathbf{r}, \tau)]}, \quad (33)$$

where $n_0 = 1/a_x a_y$.

B. Review of the RG analysis

Before proceeding with our replica analysis, we review the highlights of the perturbative RG analysis previously undertaken by some of us¹⁷ to set the stage for our expectations for the results. In the RG approach, one performs momentum shell integrals for large (absolute values of) frequency and q_y , rescales the lengths and times to keep the cutoffs fixed, and then examines how the parameters of the theory evolve under this transformation. The power of this approach is that it may be carried out perturbatively in the disorder, allowing one to avoid the subtleties that arise from the employment of replicas or other methods needed to handle disorder averages when $V(\mathbf{r})$ remains in the exponent.

Another useful feature of the RG approach is that it allows one to look at the contributions to the impurity action individually. Specifically, one must modify Eq. (33) to read

$$S'_{\text{imp}} = n_0 \int d\mathbf{r} d\tau V(\mathbf{r}) \sum_{\mathbf{K} \neq 0} \Delta_{\mathbf{K}}(l) e^{i\mathbf{K} \cdot [\mathbf{r} - \mathbf{u}(\mathbf{r}, \tau)]}, \quad (34)$$

where l is the standard scaling variable and $\Delta_{\mathbf{K}}(l=0) = 1$. The behavior of $\Delta_{\mathbf{K}}(l)$ is different depending on whether \mathbf{K} is parallel or perpendicular to the stripes. For \mathbf{K} *parallel* to the stripes, one finds

$$\frac{d\Delta_{\mathbf{K}}(l)}{dl} = \left(\frac{1 - \gamma_{\mathbf{K}}}{2} \right) \Delta_{\mathbf{K}}, \quad (35)$$

with $\gamma_{\mathbf{K}}$ increasing for increasing K , and taking the value

$$\gamma_{\mathbf{K}} = \frac{a_x l_B^2}{a_y} \sum_{q_x} dq_x \frac{d_{xx}(q_x)}{\sqrt{d_{xx}(q_x) d_{yy}(q_x) - d_{xy}^2(q_x)}} - 2, \quad (36)$$

for $\mathbf{K} = K_{y0}\hat{y}$, i.e., for the shortest wavevector parallel to the stripes. The form of Eq. (34) indicates that the stripes can undergo a quantum phase transition, from one in which they are pinned for motion parallel to the stripes ($\Delta_{\mathbf{K}=(2\pi/a_y)\hat{y}}$ relevant) to one in which they are unpinned ($\Delta_{\mathbf{K}=(2\pi/a_y)\hat{y}}$ irrelevant) and free to slide. As can be seen from Eq. (36), which state the system ends up in depends in detail on the elastic stiffness of the stripes. For the $N = 3$ Landau level, using the same matching procedure as we described above, it was found that the stripes undergo a quantum depinning transition around $\Delta\nu \approx 0.43$ for very weak disorder, with the unpinned state occurring for the larger values of $\Delta\nu$. From the form of Eq. (34), one can see the depinning occurs via a KT transition¹⁷.

The RG analysis is more complicated if \mathbf{K} is perpendicular to the stripes. In this case, for any $\mathbf{K} = (K_x, 0)$, the free energy $F \equiv -\ln \int \mathcal{D}\mathbf{u} \exp(-S_0 - S'_{\text{imp}})$ diverges at low temperatures as $T^{-2/5}$ for any $\Delta\nu$. This indicates that pinning *perpendicular* to the stripes is always relevant. Our interpretation of this is that the stripes will be trapped

in channels; however, they are still free to move along the channels so that this would not spoil the phase transition described above.

The perturbative RG thus leads us to expect a quantum phase transition from a pinned to an unpinned state as $\Delta\nu$ increases towards $1/2$. We will see that the replica analysis discussed below bears out this expectation, and gives results very much in harmony with those of the perturbative RG.

Before closing this section, we believe it is important to point out that different methods for estimating the dynamical matrix $D_{\alpha\beta}$ will lead to different values of $\gamma_{\mathbf{K}}$, and may ultimately lead to different conclusions regarding whether there is a depinning transition in this system. Specifically, calculations based on edge state models for the low energy states of the stripes^{8,25} lead to estimates in which the stripes are always in the pinned phase for all $\Delta\nu \neq 1/2$. This difference does *not* come as a result of a fundamental difference in the assumed degrees of freedom for the underlying low-energy model; indeed, one may show the edge state and disordered solid models can be mapped onto one another^{8,28}. The difference arises purely as a result of the different estimates one arrives at for the dynamical matrix using the two different approaches.

A convincing argument has been made⁸ in the context of the edge state model that the stripes should be in the pinned state provided the system preserves particle-hole symmetry at $\Delta\nu = 1/2$. This is not the situation for the model we have adopted: by modeling the stripes as quantum disordered crystals, we assume the system is isomorphic to one in which the system is composed of point particles, which does not have this symmetry. This is natural for our starting point, the modulated stripe HF ground state. These states are highly reminiscent of a collection of electrons in wavepackets, and it is natural to suppose the low-energy fluctuations will consist of displacements of these wavepackets. Moreover, the HF groundstates from which we start *spontaneously* breaks particle-hole symmetry at $\Delta\nu = 1/2$, arriving at a lower energy state than the uniform, particle-hole symmetric one. Although the sliding fluctuations modify the density to one where the particle-hole symmetry breaking may not be immediately apparent, one does expect to see the broken symmetry in pair correlation functions. Since our estimates of the dynamical matrix elements are taken from the density-density response function, which is closely related to the pair correlation function, it is not surprising that our final result does not respect the limit set by particle-hole symmetry.

An interesting aspect of our approach is that it predicts, in the clean limit, that there will be *two* smectic states, a particle-like one, and a hole-like one, at $\Delta\nu = 1/2$. The transition between them as a function of $\Delta\nu$ will presumably be first order. While a direct experimental confirmation of this is difficult, the predictions we make in the present study – a depinning transition, and a dynamical conductivity whose form is characteristic of a depinned state – offer a falsifiable test of whether the QH smectic actually breaks particle-hole symmetry: should experiments show that the dynamical conductivity unambiguously displays behavior associated with the depinned state, then it is most likely that the QH smectic indeed spontaneously breaks particle-hole symmetry at $\Delta\nu = 1/2$.

IV. BEYOND PERTURBATION THEORY: REPLICAS AND THE GVM

When a perturbation is relevant in an RG analysis, it is necessary to develop some method for approximating the action to which the system is flowing in order to compute properties of the system. For a pinned elastic system, replicas combined with the Gaussian variational method (GVM) make this possible. In this section, we briefly introduce this method, and go on to discuss some aspects of its application to the stripe system. A fuller discussion may be found in Refs. 20–23.

A. Basic equations

The fundamental idea of the GVM is to replace a complicated action S with a variational action S_{var} that is *quadratic*, with coefficients chosen to best match the original problem. This is accomplished by minimizing a free energy²³

$$F_{\text{var}} = F_0 + T [\langle S \rangle_{S_{\text{var}}} - \langle S_{\text{var}} \rangle_{S_{\text{var}}}], \quad (37)$$

where S_{var} is the quadratic variational action, F_0 is the free energy associated with that action, and here $\langle \dots \rangle_{S_{\text{var}}}$ indicates a functional integral over displacements, with S_{var} as a weighting. For our problem, we would like to disorder average F_{var} , a difficult task because the disorder potential V enters F_{var} in a complicated and analytically intractable way. A standard method for dealing with this is the replica trick³¹, in which one creates n copies of the original action, computes the replicated partition function Z^n , and then takes the $n \rightarrow 0$ limit. The identity $F = \lim_{n \rightarrow 0} (1 - Z^n)/n$ connects the disorder-averaged, replicated partition function to the free energy. In practice, one first replicates both the Gaussian variational free energy and the original action, performs the disorder average on Z^n , and then applies Eq. 37 to the resulting replicated effective action, taking the $n \rightarrow 0$ limit only after finding the equations that come from minimizing F_{var} .

Following this program, the effective replicated action after disorder averaging is defined by

$$\exp(-S_{\text{eff}}) = \frac{1}{\int DV P(V)} \int DV P(V) \exp \left\{ - \sum_{a=1}^n \left[S_0^{(a)} + S'_{\text{imp}}^{(a)} \right] \right\}, \quad (38)$$

which yields

$$S_{\text{eff}} = S_0^{(\text{eff})} + S_{\text{imp}}^{(\text{eff})}, \quad (39)$$

$$S_0^{(\text{eff})} = \frac{1}{2T} \sum_{a=1}^n \sum_{\mathbf{q}, \omega_n} \sum_{\alpha, \beta=x, y} u_{\alpha}^a(\mathbf{q}, \omega_n) G_{\alpha\beta}^{(0)-1}(\mathbf{q}, \omega_n) u_{\beta}^a(-\mathbf{q}, -\omega_n), \quad (40)$$

$$S_{\text{imp}}^{(\text{eff})} \simeq -v_{\text{imp}} \sum_{a,b=1}^n \int_0^{1/T} d\tau_1 \int_0^{1/T} d\tau_2 \int d\mathbf{r} \sum_{\mathbf{K} \neq 0} \cos[\mathbf{K} \cdot [\mathbf{u}^a(\mathbf{r}, \tau_1) - \mathbf{u}^b(\mathbf{r}, \tau_2)]], \quad (41)$$

where $v_{\text{imp}} = V_0^2 a_x^2 a_y^2 n_0^2$, and a, b are replica indices that run from 1 to n . In obtaining the last line of Eq. (41) we have neglected some rapidly oscillating terms.

In the pure limit the action is diagonal in the replica indices. Disorder averaging introduces coupling among the replicas through the impurity coupling $S_{\text{imp}}^{(\text{eff})}$ in Eq. (41). This coupling is non-Gaussian, so we next apply the GVM. We introduce the Gaussian variational action S_{var} which takes the form

$$S_{\text{var}} = \frac{1}{2T} \sum_{\mathbf{q}, \omega_n} u_{\alpha}^a(\mathbf{q}, \omega_n) (G^{-1})_{\alpha\beta}^{ab}(\mathbf{q}, \omega_n) u_{\beta}^b(-\mathbf{q}, -\omega_n), \quad (42)$$

where $G_{\alpha\beta}^{ab}(\mathbf{q}, \omega_n)$ is the displacement Green's function,

$$G_{\alpha\beta}^{ab}(\mathbf{q}, \omega_n) = \int_0^{1/T} d\tau \langle T_{\tau} u_{\alpha}^a(\mathbf{q}, \tau) u_{\beta}^b(-\mathbf{q}, 0) \rangle_{S_{\text{var}}}. \quad (43)$$

This quantity is to be determined through minimization of the free energy. It is convenient to write it in terms of the bare Green's function via

$$(G^{-1})_{\alpha\beta}^{ab}(\mathbf{q}, \omega_n) = G_{\alpha\beta}^{(0)-1}(\mathbf{q}, \omega_n) \delta_{ab} - \hat{\zeta}_{\alpha\beta}^{ab}(\omega_n), \quad (44)$$

where $\hat{\zeta}_{\alpha\beta}^{ab}(\omega_n)$ is the element of the variational self-energy matrix $\hat{\zeta}$ (here and hereafter the ‘‘hat’’ indicates that the quantity is a 2×2 matrix). Note that there is no \mathbf{q} dependence in $\hat{\zeta}$ because we have chosen our impurity action to be local in space; this will become clear when we find the saddle point equations below. Note also the obvious symmetries $G^{ab} = G^{ba}$ and $\zeta^{ab} = \zeta^{ba}$.

Substituting $S = S_{\text{eff}}$ into Eq. (37) and performing the functional integrals, one finds

$$F_{\text{var}} = F_0 + T \left[\langle S_0^{(\text{eff})} \rangle_{S_{\text{var}}} + \langle S_{\text{imp}}^{(\text{eff})} \rangle_{S_{\text{var}}} - \langle S_{\text{var}} \rangle_{S_{\text{var}}} \right], \quad (45)$$

where

$$F_0 = -\frac{1}{2} T \text{Tr} \ln \hat{G} + \text{const.}, \quad (46)$$

$$\langle S_0^{(\text{eff})} - S_{\text{var}} \rangle_{S_{\text{var}}} = \frac{1}{2} \sum_{\mathbf{q}, \omega_n} \sum_{a,b=1}^n \sum_{\alpha, \beta=x, y} \left[G_{\alpha\beta}^{(0)-1}(\mathbf{q}, \omega_n) \delta_{ab} - (G^{-1})_{\alpha\beta}^{ab}(\mathbf{q}, \omega_n) \right] G_{\alpha\beta}^{ba}(\mathbf{q}, \omega_n), \quad (47)$$

$$\langle S_{\text{imp}}^{(\text{eff})} \rangle_{S_{\text{var}}} = -\frac{v_{\text{imp}}}{T} \sum_{a,b=1}^n \sum_{\mathbf{K} \neq 0} \int_0^{1/T} d\tau \exp \left[-\frac{1}{2} \sum_{\alpha\beta} K_{\alpha} K_{\beta} B_{\alpha\beta}^{ab}(\tau) \right], \quad (48)$$

with

$$B_{\alpha\beta}^{ab}(\tau) = \langle T_{\tau} [u_{\alpha}^a(\mathbf{r}, \tau) - u_{\beta}^b(\mathbf{r}, 0)]^2 \rangle_{S_{\text{var}}} = T \sum_{\mathbf{q}, \omega_n} \left[G_{\alpha\beta}^{aa}(\mathbf{q}, \omega_n) + G_{\alpha\beta}^{bb}(\mathbf{q}, \omega_n) - 2 \cos(\omega_n \tau) G_{\alpha\beta}^{ab}(\mathbf{q}, \omega_n) \right]. \quad (49)$$

B. Saddle point equations

Equation (37) next needs to be extremized, which is accomplished by taking derivatives with respect to the matrix elements of G , $\partial F_{\text{var}}/\partial \hat{G} = 0$. The resulting saddle point equations (SPE's) are most easily expressed in terms of the self-energy matrix as^{21,22}

$$\zeta_{\alpha\beta}^{aa}(\omega_n) = 4v_{\text{imp}} \int_0^{1/T} d\tau \left\{ (1 - \cos \omega_n \tau) V'_{\alpha\beta} [B^{aa}(\tau)] + \sum_{b \neq a} V'_{\alpha\beta} [B^{ab}(\tau)] \right\}, \quad (50)$$

$$\zeta_{\alpha\beta}^{a(b \neq a)}(\omega_n) = -4v_{\text{imp}} \int_0^{1/T} d\tau \cos \omega_n \tau V'_{\alpha\beta} [B^{ab}(\tau)], \quad (51)$$

where

$$V'_{\alpha\beta} [B^{ab}(\tau)] = \sum_{\mathbf{K} \neq 0} K_\alpha K_\beta \exp \left[-\frac{1}{2} \sum_{\mu\nu=x,y} K_\mu K_\nu B_{\mu\nu}^{ab}(\tau) \right]. \quad (52)$$

It is apparent at this point that the self-energy has no \mathbf{q} dependence. Moreover, if we assume that reflection symmetry for the stripe system is not spontaneously broken after disorder averaging, it is clear that the solutions of interest to Eqs. (50) and (51) will satisfy $\zeta_{xy}^{ab} = 0$. Our task will be to find the self-energy matrix elements that are diagonal in the spatial indices.

It is now convenient to take $n \rightarrow 0$ limit. In doing so, the replica indices are taken to be continuous rather than integral, and they are taken from running from 1 to n to running from 1 to 0. An important aspect of taking this limit is that one *assumes* the self-energy and Green's function matrices may be written in a "hierarchical form"^{19,31}. In the limit $n \rightarrow 0$ such matrices are characterized by diagonal and off-diagonal terms, which may be written as

$$\zeta_{\alpha\alpha}^{aa} \rightarrow \tilde{\zeta}_\alpha, \quad (53)$$

$$\zeta_{\alpha\alpha}^{ab(\neq a)} \rightarrow \zeta_\alpha(u), \quad \text{for } 0 \leq u \leq 1. \quad (54)$$

Similarly, $G_{\alpha\beta}^{aa} \rightarrow \tilde{G}_{\alpha\beta}$, $G_{\alpha\beta}^{ab(\neq a)} \rightarrow G_{\alpha\beta}(u)$ ($0 \leq u \leq 1$). Since the disorder potential $V(\mathbf{r})$ is time independent, a further simplification one finds is that the off-diagonal replica components $\zeta_{\alpha\alpha}^{ab(\neq a)}$ and $G_{\alpha\beta}^{ab(\neq a)}$ are τ independent,^{21,22,24} so that $\hat{G}(\mathbf{q}, \omega_n, u)$ and $\hat{\zeta}(\mathbf{q}, \omega_n, u)$ are different than zero only for $\omega_n = 0$:

$$\hat{G}(\mathbf{q}, \omega_n, u) = \hat{G}(\mathbf{q}, u) \delta_{\omega_n, 0}, \quad (55)$$

$$\hat{\zeta}(\omega_n, u) = \hat{\zeta}(u) \delta_{\omega_n, 0}. \quad (56)$$

The SPE's (50) and (51) now may be written as

$$\tilde{\zeta}_\alpha(\omega_n) = \int_0^1 du \zeta_\alpha(u) + 4v_{\text{imp}} \int_0^{1/T} d\tau (1 - \cos(\omega_n \tau)) V'_{\alpha\alpha} [\tilde{B}(\tau)], \quad (57)$$

$$\zeta_\alpha(u) = -\frac{4v_{\text{imp}}}{T} V'_{\alpha\alpha} [B(u)], \quad (58)$$

where, from Eq. (49),

$$\tilde{B}_{\mu\mu}(\tau) = 2T \sum_{\mathbf{q}, \omega_n} (1 - \cos(\omega_n \tau)) \tilde{G}_{\mu\mu}(\mathbf{q}, \omega_n), \quad (59)$$

$$\begin{aligned} B_{\mu\mu}(u) &= 2T \sum_{\mathbf{q}} \left\{ \left[\sum_{\omega_n} \tilde{G}_{\mu\mu}(\mathbf{q}, \omega_n) \right] - G_{\mu\mu}(\mathbf{q}, u) \right\} \\ &= 2T \sum_{\mathbf{q}} \left\{ \left[\tilde{G}_{\mu\mu}(\mathbf{q}, \omega_n = 0) - G_{\mu\mu}(\mathbf{q}, u) \right] + \sum_{\omega_n \neq 0} \tilde{G}_{\mu\mu}(\mathbf{q}, \omega_n) \right\}. \end{aligned} \quad (60)$$

Note that Eq. (57) also gives us

$$\tilde{\zeta}_\alpha(\omega_n = 0) = \int_0^1 du \zeta_\alpha(u). \quad (61)$$

To solve the Eqs. (57) and (58) we must know the relation between $\tilde{G}(\omega_n)$, $G(u)$ and $\tilde{\zeta}(\omega_n)$ and $\zeta(u)$. Eqs. (55) and (56) indicate that

$$\tilde{G}_{\mu\mu}(\mathbf{q}, \omega_n \neq 0) = \left[\hat{G}^{(0)-1}(\mathbf{q}, \omega_n) - \hat{\zeta}(\omega_n) \right]_{\mu\mu}^{-1}. \quad (62)$$

The quantities $\hat{G}(\mathbf{q}, \omega_n = 0)$ and $\hat{G}(u)$ are related to $\hat{\zeta}(\omega_n = 0)$ and $\hat{\zeta}(u)$ through inversion rules that generalize the inversion of an $n \times n$ hierarchical matrix to the $n \rightarrow 0$ limit. The inversion rules for a simple hierarchical matrix are well-known^{20,31}, and their generalization to a situation in which the elements of the hierarchical matrix are proportional to the unit matrix – which would be the case for our matrices if the elastic system were isotropic – is trivial. However, in our case the entries of the hierarchical matrix are 2×2 matrices with a non-trivial structure. Moreover, the perturbative RG indicates we should expect the pinning properties perpendicular and parallel to the stripes to be different, and we need to generalize the inversion rules to allow for this possibility. With some work, the most general inversion rules for our situation can be derived analytically, and we present this derivation in Appendix B. According to Eq. (B16), the Green's functions are related to the self-energy by

$$\hat{G}(\mathbf{q}, \omega_n = 0) - \hat{G}(\mathbf{q}, u) = \left[\hat{D}(\mathbf{q}) - \hat{\zeta}(\omega_n = 0) + \hat{\zeta}(u) \right]^{-1} + \int_u^1 dv \left[\hat{D}(\mathbf{q}) + [\hat{\zeta}](v) \right]^{-1} \cdot \hat{\zeta}'(v) \cdot \left[\hat{D}(\mathbf{q}) + [\hat{\zeta}](v) \right]^{-1}, \quad (63)$$

where $\hat{\zeta}'(v) = d\hat{\zeta}(v)/dv$, and

$$[\hat{\zeta}](u) = u \hat{\zeta}(u) - \int_0^u dv \hat{\zeta}(v). \quad (64)$$

Once we have obtained the self-energy, we can compute the finite-frequency conductivities in Eq. (27) by analytically continuing to real frequency in Eq. (62), so that

$$\tilde{G}_{\mu\mu}^{\text{ret}}(\mathbf{q}, \omega \neq 0) = \left[\hat{G}_{\text{ret}}^{(0)-1}(\mathbf{q}, \omega) - \hat{\zeta}^{\text{ret}}(\omega) \right]_{\mu\mu}^{-1}. \quad (65)$$

Inserting Eq. (65) into Eq. (27) we arrive at the longitudinal conductivity

$$\sigma_{\alpha\alpha}(\omega) = \frac{e^2}{a_x a_y} \frac{i\omega \tilde{\zeta}_{\bar{\alpha}}^{\text{ret}}(\omega)}{\tilde{\zeta}_x^{\text{ret}}(\omega) \tilde{\zeta}_y^{\text{ret}}(\omega) - \omega^2 / l_B^4}, \quad (66)$$

where $\bar{\alpha} = y(x)$ for $\alpha = x(y)$.

To obtain $\tilde{\zeta}_{\bar{\alpha}}^{\text{ret}}(\omega)$, we analytically continue Eq. (57). As shown in Appendix C, this results in the equation (for $T = 0$)

$$\tilde{\zeta}_{\bar{\alpha}}^{\text{ret}}(\omega) = e_{\bar{\alpha}} - 4v_{\text{imp}} \sum_{\mathbf{K} \neq 0} K_{\bar{\alpha}}^2 \int_0^{\infty} dt (e^{i\omega t} - 1) \text{Im} [I(t, K_x) I(t, K_y)], \quad (67)$$

where

$$I(t, K_{\mu}) = \exp \left[-\frac{K_{\mu}^2}{\pi} \int_0^{\infty} df A_{\mu}(f) (1 - e^{itf}) \right], \quad (68)$$

$$A_{\mu}(f) = \sum_q \text{Im} \left[\tilde{G}_{\mu\mu}^{\text{ret}}(\mathbf{q}, f) \right], \quad (69)$$

$$e_{\alpha} = \tilde{\zeta}_{\alpha}^{\text{ret}}(0^+) = \int_0^1 du \zeta_{\alpha}(u) - 4v_{\text{imp}} \sum_{\mathbf{K} \neq 0} K_{\alpha}^2 \int_0^{\infty} dt \text{Im} [I(t, K_x) I(t, K_y)] \\ - 2v_{\text{imp}} \sum_{\mathbf{K} \neq 0} K_{\alpha}^2 \int_0^{1/T} d\tau \exp \left[-\frac{1}{2} \sum_{\mu=x,y} K_{\mu}^2 \tilde{B}_{\mu\mu}(\tau) \right]. \quad (70)$$

As we proceed with our analysis, it is helpful to keep in mind that $A_{\mu}(f)$ is a spectral function, and that $e_{\alpha} \neq 0$ is an energy offset that in a pinned state opens a gap in the phonon spectrum, as discussed more fully below. Note also that Eq. (67) indicates that $\tilde{\zeta}_{\bar{\alpha}}^{\text{ret}}(\omega)$ at each ω point depends on the whole spectrum of $A_{\alpha}(f)$, and this will be

complications that for this analysis cannot be avoided, as is the case for other pinned systems^{21,22}. Since quantum fluctuations play a crucial role in this system, it is useful for us to define effective Debye-Waller factors via

$$W(\mathbf{K}) = \frac{1}{\pi} \sum_{\mu=x,y} K_{\mu}^2 \int_0^{\infty} df A_{\mu}(f). \quad (71)$$

These quantities are a measure of the mean square displacements in units of the lattice constants, and when large they indicate that quantum fluctuations cannot be ignored in computing the dynamical conductivity. Clearly this will be the case in the vicinity of the quantum depinning transition. On the other hand, if $W(\mathbf{K})$ are small for all \mathbf{K} , one may expand the exponential function on the right-hand side of Eq. (68) and keep only the leading order term. Eqs. (67) then become greatly simplified, taking the form

$$\tilde{\zeta}_{\alpha}^{\text{ret}}(\omega) = e_{\alpha} + 2v_{\text{imp}} \sum_{\mathbf{K} \neq 0} K_{\alpha}^2 \sum_{\mu=x,y} K_{\mu}^2 \sum_{\mathbf{q}} \left[\tilde{G}_{\mu\mu}^{\text{ret}}(\mathbf{q}, \omega) - \tilde{G}_{\mu\mu}^{\text{ret}}(\mathbf{q}, \omega = 0^+) \right]. \quad (72)$$

This is called the semiclassical approximation (SCA)^{21,22}, and it presents a powerful simplification when it is valid. In particular one sees that Eq. (72) is local in the frequency, so that $\tilde{\zeta}_{\alpha}^{\text{ret}}(\omega)$ may be determined one frequency at a time. Unfortunately, the SCA is not valid in our present problem, and we are forced to solving the full SPE's (67) numerically. We will see however that the solutions have several interesting properties that give clear signatures of the depinned phase and the transition leading to it.

C. Replica symmetric (RS) solution vs replica symmetry breaking (RSB) solution

Eq. (67) shows that the replica diagonal self energy $\tilde{\zeta}_{\alpha}^{\text{ret}}(\omega)$ depends on the off-diagonal terms $\zeta_{\alpha}(u)$ through the constants e_{α} . It is instructive to first examine the possible structure of $\zeta_{\alpha}(u)$. If $\zeta_{\alpha}(u)$ is a constant in u , the symmetry of permutation of the replica indices is kept and the solution is ‘‘replica symmetric’’ (RS). On the other hand, when $\zeta_{\alpha}(u)$ varies with u , the solution displays replica symmetry breaking (RSB).

For many low-dimensional systems ($d \leq 2$), the appropriate solution to the SPE's is of the RSB type. Often there is a simple ‘‘one-step RSB’’ solution, with $\zeta(u)$ piecewise constant, but stepping up or down at a single point u_c ($0 < u_c < 1$). It follows from Eq. (64) that $[\zeta_{\alpha}](u_c) \neq 0$ in the RSB state. On the other hand, $[\zeta_{\alpha}](u_c) = 0$ for the RS solution.

Following Refs. 21 and 23, one can establish a close relation between $[\zeta_{\alpha}](u_c)$ and e_{α} . By making use of $[\zeta_{\alpha}](u_c)$, Eq. (57) can be rewritten as

$$\tilde{\zeta}_{\alpha}(\omega_n \neq 0) = [\zeta_{\alpha}](u_c) - 4v_{\text{imp}} \int_0^{1/T} d\tau (1 - \cos(\omega_n \tau)) \left\{ V'_{\alpha\alpha}[\tilde{B}(\tau)] - V'_{\alpha\alpha}[B(u_c)] \right\}. \quad (73)$$

Here, substituting $V'_{\alpha\alpha}[B(u_c)]$ from $V'_{\alpha\alpha}[\tilde{B}(\tau)]$ guarantees that as $T \rightarrow 0$ the second term of the right-hand side of Eq. (73) vanishes at $\omega_n \rightarrow 0$. Comparing Eqs. (73) and (67) one immediately concludes that

$$e_{\alpha} = -[\zeta_{\alpha}](u_c). \quad (74)$$

So $e_{\alpha} = 0$ in the RS state and $e_{\alpha} \neq 0$ in the RSB state. The two constants e_x and e_y have significant physical meanings. They may be regarded as a measure of the strength of pinning by the disorder potential and are roughly speaking proportional to the gap in the low-energy magnetophonon modes. If $e_{\alpha} = 0$, the phonon spectrum is gapless at $\mathbf{q} = 0$ indicating the system can slide as a whole without energy cost, and is not pinned. Thus an RS solution is expected in the unpinned state. If $e_{\alpha} \neq 0$ as in the RSB solution, a gap opens up in the low-energy magnetophonon modes, uniform sliding cannot be achieved at zero energy, and the system is pinned by disorder.

We will show in Sec. V that for $\Delta\nu < \Delta\nu_c$, both e_x and e_y are nonzero and the stripes are thus fully pinned. As $\Delta\nu \rightarrow \Delta\nu_c$, $e_y \rightarrow 0$, indicating a quantum depinning transition. The solution to the SPE's is RS for motion along the stripes but RSB for motion perpendicular to the stripes. We call this type of solution to the SPE's a *partial* RSB state. The detailed behavior of the system in this state will be explored in Sec. VI.

V. RESULTS FOR PINNED STATE: RSB SOLUTION

We begin by examining solutions of the SPE's for which the QH stripes are fully pinned by disorder. According to the RG result reviewed in Sec. III B, this corresponds to $\Delta\nu < \Delta\nu_c$ in which the disorder is relevant. In this case both e_x and e_y are nonzero. We begin by discussing constraints on e_x and e_y which determine their values, allowing us to solve the SPE's without explicitly solving for $\zeta_{\alpha}(u)$ and $\tilde{\zeta}_{\alpha}$. We then present numerical results for the conductivity.

A. Two constraints for e_x and e_y

The SPE's (67) become a set of closed equations if e_x and e_y are known. Formally, e_x and e_y need to be determined self-consistently by solving Eq. (58). The SPE's in fact have a family of solutions (parameterized by u_c), and determining which is best generically would be determined by minimization of the free energy. In the case of spatial dimension $d > 2$, u_c determined this way leads to $\text{Re}[\sigma(\omega)] \sim \omega^2$ at small ω . This is consistent with arguments by Mott as well as some exact solutions²⁹ (up to a logarithmic correction). However, for $d \leq 2$, this approach can yield an unphysical result in which, in the pinned state, the conductivity shows a true gap: $\text{Re}[\sigma(\omega)]$ vanishes below some gap frequency. Alternatively, one may *impose* the condition $\text{Re}[\sigma(\omega)] \sim \omega^2$ at small ω . It is known that the doing so generates an equation that may be understood as imposing a marginal stability on the so-called replicon mode²¹. Although this point is not fully understood, it is a common procedure that leads to physically reasonable results, and we will adopt it by imposing the condition $\text{Re}[\sigma_{\alpha\alpha}(\omega)] \sim \omega^2$ at small ω in the pinned state. From Eq. (66), this is equivalent to $\text{Im}[\zeta_{\alpha}^{\text{ret}}(\omega)] \sim \omega$. Note that this guarantees the magnetophonon mode density of state vanishes at zero frequency, as one should expect for a pinned system.

To obtain the explicit condition leading to $\text{Im}[\zeta_{\alpha}^{\text{ret}}(\omega)] \sim \omega$, we expand the SPE's, Eqs. (67), for small- ω . The integral over t now is dominated by the large t region. Therefore, the term $\int_0^{\infty} df A_{\mu}(f)e^{ift}$ in the argument of the exponential function in Eq. (68) must be small due to the rapidly oscillating nature of e^{ift} , leading to

$$I(t, K_x)I(t, K_y) \simeq e^{-W(\mathbf{K})} \left[1 + \frac{1}{\pi} \sum_{\mu=x,y} K_{\mu}^2 \int_0^{\infty} df A_{\mu}(f)e^{ift} \right]. \quad (75)$$

The SPE's (67) at small ω become

$$\tilde{\zeta}_{\alpha}^{\text{ret}}(\omega) \simeq e_{\alpha} + 2 \sum_{\mathbf{K} \neq 0} v(\mathbf{K}) K_{\alpha}^2 \sum_{\mu=x,y} K_{\mu}^2 \sum_q \left[\tilde{G}_{\mu\mu}^{\text{ret}}(\mathbf{q}, \omega) - \tilde{G}_{\mu\mu}^{\text{ret}}(\mathbf{q}, \omega = 0^+) \right], \quad (76)$$

where $v(\mathbf{K}) = v_{\text{imp}}e^{-W(\mathbf{K})}$. This is very similar to the SPEs (72) within the SCA except that v_{imp} in Eq. (72) is now replaced by $v(\mathbf{K})$. Apparently, when $W(\mathbf{K}) \ll 1$ the semiclassical approximation is valid, and Eq. (76) reduces to Eq. (72).

At small ω , we write

$$\text{Re} \left[\tilde{\zeta}_{\alpha}^{\text{ret}} \right] \simeq e_{\alpha}, \quad (77)$$

$$\text{Im} \left[\tilde{\zeta}_{\alpha}^{\text{ret}} \right] \simeq \beta_{\alpha}\omega, \quad (78)$$

and correspondingly $\sum_{\mathbf{q}} \tilde{G}_{\mu\mu}^{\text{ret}}(\mathbf{q}, \omega) \simeq G_{\mu 0} + \sum_{\alpha=x,y} g_{\mu\alpha}\beta_{\alpha}\omega$. The condition for nonvanishing β_{α} from Eq. (76) becomes

$$(U_{xx} - 1)(U_{yy} - 1) - U_{yx}U_{xy} = 0, \quad (79)$$

where

$$U_{\mu\nu} = 2 \sum_{\mathbf{K} \neq 0} K_{\nu}^2 v(\mathbf{K}) \sum_{\alpha=x,y} K_{\alpha}^2 g_{\alpha\mu}. \quad (80)$$

Eq. (79) is our first constraint for e_x and e_y .

The second constraint follows from the assumption of a *one-step* RSB solution in which $\zeta_{\alpha}(u < u_c) = 0$. Eqs. (74) and (64) immediately yield

$$e_{\alpha} = -u_c \zeta_{\alpha}(u_c). \quad (81)$$

Inserting Eq. (81) into Eq. (63) and noting $\zeta'_{\alpha}(v) = 0$ for $v \geq u_c$ we get

$$\widehat{\tilde{G}}(\mathbf{q}, n=0) - \widehat{G}(\mathbf{q}, u_c) = \left[\widehat{D}(\mathbf{q}) + \hat{e} \right]^{-1}, \quad (82)$$

where the elements of the matrix \hat{e} are $e_{\alpha\beta} = e_{\alpha}\delta_{\alpha\beta}$. Substituting Eq. (82) in (60) and making use of $\tilde{G}_{\mu\mu}(\mathbf{q}, \omega_n \rightarrow 0) = \left[\widehat{D}(\mathbf{q}) + \hat{e} \right]^{-1}_{\mu\mu}$ results in the equation

$$B_{\mu\mu}(u_c) = \frac{2}{\pi} \int_0^{\infty} df A_{\mu}(f), \quad (83)$$

which can be inserted in Eq. (58) to give

$$\zeta_\alpha(u_c) = \frac{4v_{imp}}{T} \sum_{\mathbf{K} \neq 0} K_\alpha^2 e^{-W(\mathbf{K})}. \quad (84)$$

Eqs. (84) and (81) lead to the ratio

$$\frac{e_y}{e_x} = \frac{\sum_{\mathbf{K} \neq 0} K_y^2 e^{-W(\mathbf{K})}}{\sum_{\mathbf{K} \neq 0} K_x^2 e^{-W(\mathbf{K})}}. \quad (85)$$

This shows that the pinning of the stripes will generically be anisotropic, and serves as our second constraint for e_α .

The appearance of the Debye-Waller factors $W(\mathbf{K})$ in Eq. (85) has a significant impact: they are responsible for the change of behavior in $\tilde{\zeta}_\alpha^{\text{ret}}(\omega)$ across the depinning transition. As we shall see, whenever $K_y \neq 0$, $W(\mathbf{K})$ increases as $\Delta\nu \rightarrow \Delta\nu_c$ from below, and it eventually diverges at $\Delta\nu_c$ leading to a suppression of e_y . We will discuss this in detail below. We stress that this behavior cannot be captured by the semiclassical approximation.

B. Numerical results

We are now in a position to solve the problem numerically. For a given pair of e_x and e_y , we use an iterative method to solve for $\tilde{\zeta}_\alpha^{\text{ret}}(\omega)$ from the SPE's (67). (Typically 20-30 iterations lead to a good convergence.) The computed $\tilde{\zeta}_\alpha^{\text{ret}}(\omega)$ are then inserted in the two constraint equations (79) and (85) to generate new values of e_α , and the entire process is repeated until we reach self-consistency. We work in the $N = 3$ Landau level, although different Landau indices should give similar results. All our calculations are obtained for a disorder level $v_{imp} = 0.0005e^4/l_B^2$. This is likely to be somewhat larger than experimental values, but we choose it for numerical convenience³⁰. We do not expect our results to qualitatively change for smaller disorder strengths. We note that the bending term in Eq. (22) plays an important role of eliminating an artificial ultraviolet divergence at large q_y , but beyond this has little effect. We choose $\kappa_b = 2$ for all the fillings since this leads to a relatively fast convergence of the SPE's, although we believe the value should be somewhat smaller (of order 1).

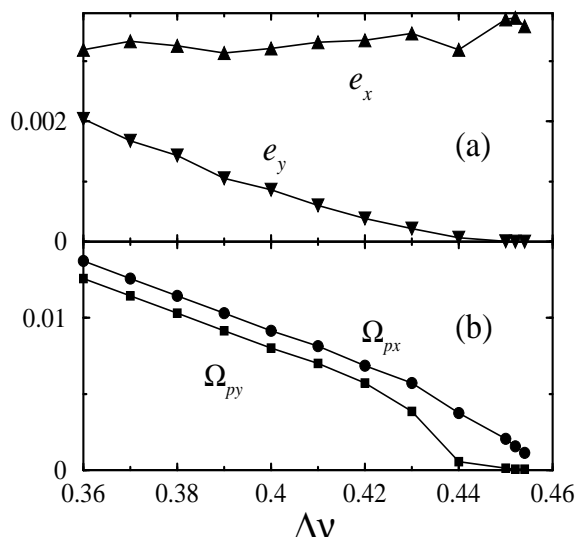


FIG. 3: (a) Constants e_x and e_y in units of e^2/l_B^3 , and (b) peak positions Ω_{px} and Ω_{py} in units of e^2/l_B , as functions of $\Delta\nu$ in the pinned state.

Results for e_x and e_y as functions of the partial filling in the pinned state are shown in Fig. 3 (a). The quantity e_x is a weak function of $\Delta\nu$, but e_y decreases with increasing $\Delta\nu$, and eventually vanishes at $\Delta\nu = \Delta\nu_c \simeq 0.459$. This is the consequence of a divergence in $W(K_x; K_y \neq 0)$ at $\Delta\nu = \Delta\nu_c$. Note $\Delta\nu_c$ is somewhat larger than what was found in the perturbative RG¹⁷. This is due to the non-vanishing disorder strength; as v_{imp} decreases, $\Delta\nu_c$ decreases to the value found in Ref. 17.

The dynamical conductivities perpendicular to the stripes in a pinned (RSB) phase are presented in Fig. 4. For $\Delta\nu$ well below $\Delta\nu_c \simeq 0.459$, $\text{Re}[\sigma_{xx}(\omega)]$ has a pinning peak whose lineshape is qualitatively similar to what is found

using the SCA.²⁴ The prominent behavior visible in Fig. 4 is a monotonic decrease of the peak frequency Ω_{px} with growing $\Delta\nu$, and its eventual collapse as the depinning transition is approached. The peak frequency behavior is more clearly shown in Fig. 3 (b). Notice the lineshape becomes increasingly asymmetric as the transition is approached. Experimental observations so far seem to be consistent with this^{15,16}.

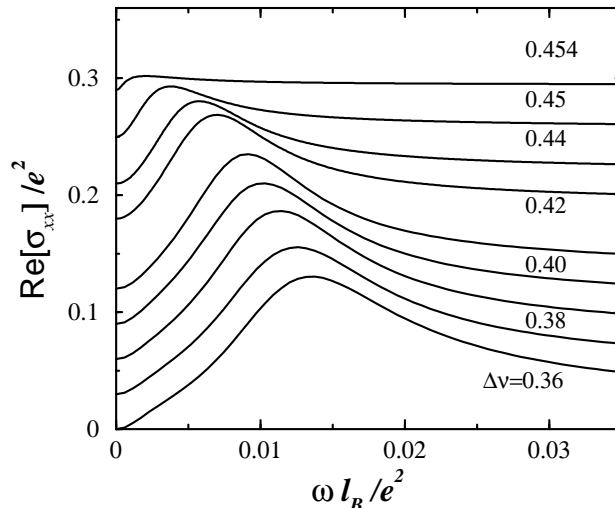


FIG. 4: Real part of conductivity perpendicular to the stripes as a function of frequency in the pinned (RSB) state. The disorder strength $v_{\text{imp}} = 0.0005e^4/l_B^2$ is used. All curves start from $\text{Re}[\sigma_{xx}(\omega)] = 0$ at $\omega = 0$, and curves except for $\Delta\nu = 0.36$ are lifted upward for clarity.

The real part of the conductivity along the stripes $\text{Re}[\sigma_{yy}(\omega)]$ is shown in Fig. 5. It also presents a pinning peak whose frequency Ω_{py} falls down with increasing $\Delta\nu$ as shown in Fig. 3 (b). But the observed peak lineshape is more interesting than that of $\text{Re}[\sigma_{xx}(\omega)]$. Below the peak frequency Ω_{py} , in the range $e_y < \omega < \Omega_{py}$ the conductivity appears to tend toward a non-vanishing value when $\Delta\nu$ is sufficiently below $\Delta\nu_c$; only for ω well below this range does one find $\text{Re}[\sigma_{yy}(\omega)]$ decreasing. The reason for this is that the quantity e_y turns out to be rather small [as shown in Fig. 3 (a)] due to a large Debye-Waller factor, and in this frequency range the system displays a behavior similar to an incoherent metal response³². We discuss this in more detail for the depinned (PRSB) phase below. For $\omega \ll e_y$, $\text{Re}[\sigma_{yy}(\omega)]$ vanishes quadratically with ω (not visible on the scale of Fig. 5), as required for a pinned state. As $\Delta\nu \rightarrow \Delta\nu_c$, we eventually reach a situation in which e_y and Ω_{py} are of similar order, in which case the pinning peak sharpens and grows quite large. This peak continuously evolves into a δ -function at zero frequency as the system enters into the PRSB state, so that the transition from pinned to depinned behavior is very continuous.

Interestingly, as shown in Fig. 3, $e_y \rightarrow 0$ governs the vanishing of both Ω_{px} and Ω_{py} . To understand this, we note that there are two gapless collective modes in the absence of the magnetic field; the magnetic field mixes them into two other modes, one of which is at a high value (order of $\hbar\omega_c$), leaving the other (magnetophonon) mode as the only gapless one. It is this single mode that responds to the electric field, albeit in an anisotropic manner in the \hat{x} and \hat{y} directions. Technically, at $\omega \sim \Omega_{px}, \Omega_{py}$, $\zeta_\alpha^{\text{ret}}(\omega)$ obeys Eqs. (77-78), and the longitudinal conductivities in Eq. (66) become

$$\text{Re}[\sigma_{\alpha\alpha}(\omega)] \simeq \frac{e^2}{a_x a_y} \omega^2 \frac{e_{\bar{\alpha}}(e_x \beta_y + e_y \beta_x) + \beta_{\bar{\alpha}} [(1 + \beta_x \beta_y) \omega^2 - e_x e_y]}{[(1 + \beta_x \beta_y) \omega^2 - e_x e_y]^2 + \omega^2 [e_x \beta_y + e_y \beta_x]^2}. \quad (86)$$

From this we can extract

$$\Omega_{px} \sim \Omega_{py} \sim \sqrt{\frac{e_x e_y}{1 + \beta_x \beta_y}}. \quad (87)$$

VI. RESULTS FOR DEPINNED STATE: PARTIAL RSB (PRSB) SOLUTION

For $\Delta\nu \geq \Delta\nu_c$ the state is characterized by $e_x \neq 0$ but $e_y = 0$. As discussed in Sec. IV.C, this corresponds to a RSB solution for $\zeta_x(u)$ but a RS solution for $\zeta_y(u)$. We call this the *PRSB* state. This state has various interesting properties that we will present below.

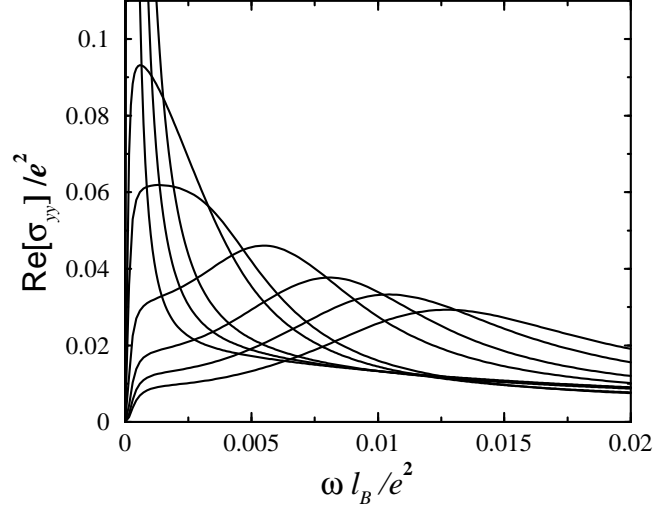


FIG. 5: Real part of conductivity along the stripes as a function of frequency in the pinned (RSB) state. The v_{imp} is the same as in Fig. 4. Curves from right to left correspond to $\Delta\nu = 0.36, 0.38, 0.4, 0.42, 0.43, 0.44, 0.45, 0.452, 0.454$, respectively.

A. Power law behavior for $\tilde{\zeta}_y^{\text{ret}}(\omega)$

From the results of the perturbative RG, we expect the stripes to remain pinned for motion in the \hat{x} direction even as the stripes become depinned for motion in the \hat{y} direction. We therefore assume that in the PRSB state, the small- ω asymptotic behavior of $\tilde{\zeta}_x^{\text{ret}}(\omega)$ remains the same as that in the RSB state [Eqs. (77-78)], and this turns out to yield a self-consistent solution. However, $\tilde{\zeta}_y^{\text{ret}}(\omega)$ is qualitatively different in the depinned state. To see this explicitly we examine the SPEs (67) for $\tilde{\zeta}_y^{\text{ret}}(\omega)$,

$$\tilde{\zeta}_y^{\text{ret}}(\omega) = -4v_{\text{imp}} \left\{ 2K_{y0}^2 \int_0^\infty dt (e^{i\omega t} - 1) \text{Im} [I(t, K_{y0})] + 4K_{y0}^2 \int_0^\infty dt (e^{i\omega t} - 1) \text{Im} [I(t, K_{y0})I(t, K_{x0})] \right\}. \quad (88)$$

There is a self-consistent solution for this equation in which $\tilde{\zeta}_y^{\text{ret}}(\omega)$ has an anomalous power law behavior at low frequencies,

$$\text{Re} \left[\tilde{\zeta}_y^{\text{ret}}(\omega) \right] \simeq \alpha_y \omega^2, \quad (89)$$

$$\text{Im} \left[\tilde{\zeta}_y^{\text{ret}}(\omega) \right] \simeq \beta_y \omega^{\gamma+1}. \quad (90)$$

This solution is only valid when

$$\gamma \geq 1, \quad (91)$$

where γ is defined in Eq. (96) below. Note that at small ω , $\tilde{\zeta}_y^{\text{ret}}(\omega)$ is dominated by large- t behavior of the integrands in Eq. (88), and this in turn depends on small- f asymptotics of $A_\alpha(f) (1 - e^{itf})$ in $I(t, K_{\alpha 0})$ [see Eq. (68)]. Making use of Eqs. (77-78) and (89-90), and of the smectic form of the dynamical matrix $\hat{D}(\mathbf{q})$ in Eqs. (22-24) (with the bending term neglected), we obtain

$$A_y(f) \simeq \frac{a_x a_y}{(2\pi)^2} \int dq_x [d_{xx}(q_x) - e_x] \text{Im} \left[\int_{-\infty}^\infty \frac{dq_y}{g_x(q_x)q_y^2 - (1 + \alpha_y)(f + i0^+)^2} \right] \simeq \frac{\pi c_v}{f}, \quad (92)$$

where

$$g_x(q_x) = (1 + \alpha_y) \{ [d_{xx}(q_x) - e_x] d_{yy}(q_x) - d_{xy}^2(q_x) \}, \quad (93)$$

and

$$c_v = \frac{a_x a_y l_B^2}{(2\pi)^2} \int dq_x \frac{d_{xx} - e_x}{\sqrt{g_x(q_x)}}. \quad (94)$$

The quantity A_y bears a singular $1/f$ term which is responsible for the unusual feature of $\tilde{\zeta}_y^{\text{ret}}(\omega)$. In contrast, $A_x(f)$ can be easily shown to converge to a constant at small f . Therefore, in Eq. (88), the large t behavior of $I(t, K_{y0})I(t, K_{x0})$ is dominated by $I(t, K_{y0})$, and the two terms within the braces have qualitatively the same small- ω behavior. Substituting Eq. (92) in Eq. (68) leads to

$$I(t, K_{y0}) \sim (1 + it\Lambda_\omega)^{\gamma+2}, \quad (95)$$

where

$$\gamma = \frac{K_{y0}^2 c_v}{\pi} - 2. \quad (96)$$

Here Λ_ω is a high-energy cutoff of order the magnetophonon band width. Inserting Eq. (95) into Eq. (88) and keeping only the leading-order terms in ω we produce Eqs. (89-90) provided Eq. (91) is met. For larger values of γ , the solution is not self-consistent, and one must revert to the full RSB (pinned) solution.

Equations (89-91) are the criteria for the existence of a PRSB solution. The inequality (91) defines a critical value $\gamma_c = 1$. Since γ in Eq. (96) increases monotonically with $\Delta\nu$, this critical value corresponds to a critical filling $\Delta\nu_c$. Our numerical result shown below in Sec. VI C indicates that $\Delta\nu_c$ obtained this way matches nicely with the critical filling defined in the RSB state through the collapse of the pinning peaks. One can also see that in the vanishing disorder limit ($e_x, \alpha_y \rightarrow 0$), γ reduces to γ_0 defined in Eq. (36) that occurs in the RG flow equation (34), and the condition (91) matches the RG condition for the irrelevance of the disorder. Technically, the reason these coincide originates from the similar ways in which the Green's function enters in the SPE (88) and in the calculation of the scaling dimension of the impurity term in the RG analysis. The minor difference is that the GVM includes the renormalization of the Green's function by disorder, while the RG analysis, being perturbative, uses the Green's function for the pure system.

In both the RSB and the PRSB states, $\text{Im}[\tilde{\zeta}_y^{\text{ret}}(\omega)]$ shows power-law behavior $\text{Im}[\tilde{\zeta}_y^{\text{ret}}(\omega)] \sim \omega^{\gamma_{\zeta y}}$ [Eqs. (78) and (90)], although the exponent is fixed at 1 for the RSB state. Plotting $\gamma_{\zeta y}$ as a function of the partial filling in Fig. 6 (a), we see that $\gamma_{\zeta y}$ *jumps* from 1 in the RSB state to 2 in the PRSB state. This jump arises from an underlying jump in the low-frequency exponent in $\text{Re}[\tilde{\zeta}_y^{\text{ret}}(\omega)]$ (from 0 in the RSB state [Eq. (77)] to 2 in the PRSB state [Eq. (89)]). Such jumps are typical for a KT-type phase transition. In the next subsection we will show the corresponding jumps in the low-frequency exponents in conductivities.

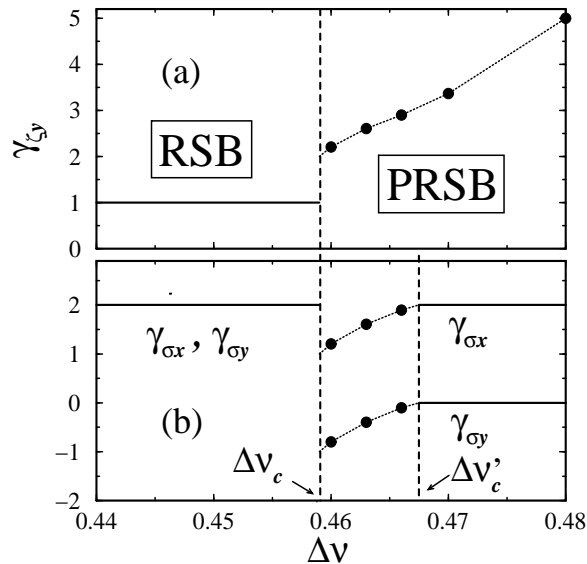


FIG. 6: Low-frequency exponents (a) $\gamma_{\zeta y}$ of $\text{Im}[\tilde{\zeta}_y^{\text{ret}}]$, and (b) $\gamma_{\sigma x}$ of $\text{Re}[\sigma_{xx}(\omega)]$ and $\gamma_{\sigma y}$ of $\text{Re}[\sigma_{yy}(\omega)]$, as functions of the partial filling $\Delta\nu$. v_{imp} is the same as in Fig. 4. $\Delta\nu_c \simeq 0.459$ marks the quantum depinning transition point and $\Delta\nu'_c$ corresponds to the second transition point at which the system changes its behavior from divergent as $\omega \rightarrow 0$ to metallic. Circles are the numerical result.

B. Anomalous low-frequency exponents for conductivities

The unusual low-frequency exponents of $\tilde{\zeta}_y^{\text{ret}}(\omega)$ directly affect the low-frequency behavior of the conductivities. Inserting Eqs. (77-78) and (89-90) in Eq. (66) we find that at small ω ,

$$\text{Re}[\sigma_{yy}(\omega)] \simeq e^2 [s_{y0} \delta(\omega) + s_{y1} \omega^{\gamma-2} + s_{y2}], \quad (97)$$

$$\text{Re}[\sigma_{xx}(\omega)] \simeq e^2 [s_{x1} \omega^\gamma + s_{x2} \omega^2], \quad (98)$$

where $s_{y0} = \Delta\nu e_x/2(1 - e_x \alpha_y)$, $s_{y1} = e_x^2 \beta_y \Delta\nu/2\pi$, $s_{y2} = \beta_x(1 + e_x \alpha_y) \Delta\nu/2\pi$, $s_{x1} = \beta_y(1 + e_x \alpha_y) \Delta\nu/2\pi$, $s_{x2} = \alpha_y^2 \beta_x \Delta\nu/2\pi$. The most significant feature in $\text{Re}[\sigma_{yy}(\omega)]$ lies in the δ peak at $\omega = 0$ ³⁴. Physically, this means that the PRSB phase is a superconducting state, and the system manages to find an effective *free* path to slide along the stripes. By contrast, $\text{Re}[\sigma_{xx}(\omega \rightarrow 0)] = 0$, implying the system is insulating for motion perpendicular to the stripes. This suggests that the PRSB state has *infinite* anisotropy in the DC conductivity. This is not observed in DC transport experiments⁵, and we comment in Sec. VIII on what is missing from our model that we believe leads to this discrepancy.

The other two terms in Eq. (97) and the terms in Eq. (98) imply an incoherent contribution at $\omega \neq 0$. Interestingly, these terms compete with each other in determining the low-frequency exponents of the conductivities, leading to a second transition. For $1 \leq \gamma < 2$, the second term in Eq. (97) and the first term in Eq. (98) dominate, so that $\text{Re}[\sigma_{yy}(\omega)] \sim \omega^{-(2-\gamma)}$ which diverges as $\omega \rightarrow 0$ ³⁵. This is a very unusual finite frequency response, which arises from the form of the Green's function in the PRSB state and so appears to be specific to this system just after the depinning transition. The response perpendicular to the stripes is insulating but also anomalous, $\text{Re}[\sigma_{xx}(\omega)] \sim \omega^\gamma$ with γ non-integer. Since γ increases with the filling $\Delta\nu$, the low-frequency exponents of $\text{Re}[\sigma_{yy}(\omega)]$ and $\text{Re}[\sigma_{xx}(\omega)]$ evolve (continuously) from $\Delta\nu_c$ (for which $\gamma = 1$) to a second critical filling $\Delta\nu'_c$ (for which $\gamma = 2$). As $\Delta\nu$ further increases from $\Delta\nu'_c$, γ becomes larger than 2, and the third term in Eq. (97) and the second term in Eq. (98) dominate the low frequency behavior. Consequently, $\text{Re}[\sigma_{yy}(\omega)] \sim \text{const.}$ for small but non-vanishing ω , which is a standard finite frequency response for a superconductor, sometimes called “incoherent metallic behavior”³². Furthermore, $\text{Re}[\sigma_{xx}(\omega)] \sim \omega^2$ which is similar to the behavior in the fully pinned state. Thus, at $\Delta\nu'_c$, the system experiences a second transition in which the finite-frequency behavior of the stripes changes. The conductivities thus have a very unusual low-frequency behavior for a small window of filling factors, $\Delta\nu_c < \Delta\nu < \Delta\nu'_c$. Interestingly, such changes in power-law behavior above a KT transition is known to occur in other contexts³⁶. The qualitative result of the low-frequency exponents $\gamma_{\sigma\alpha}$ of $\text{Re}[\sigma_{\alpha\alpha}(\omega)]$ discussed here can be seen in Fig. 6 (b). The numerical values of $\Delta\nu_c$ and $\Delta\nu'_c$ for our calculations will be discussed in the next subsection. As also shown in Fig. 6 (b), both $\gamma_{\sigma x}$ and $\gamma_{\sigma y}$ jump at the depinning transition point $\Delta\nu_c$.

In practice, the visibility of the various terms in Eqs. (97) and (98) depends on the relative size of the coefficients of each term, which we discuss in the next subsection.

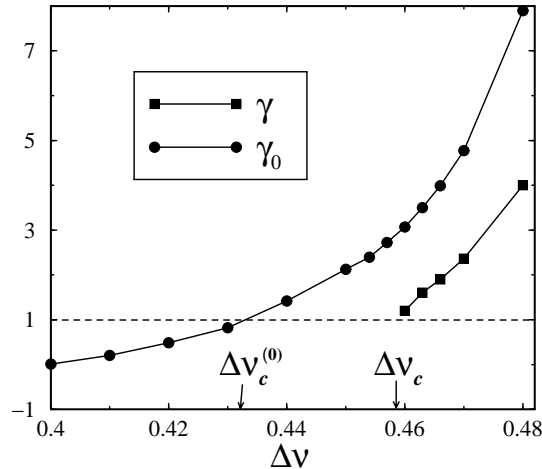


FIG. 7: Exponents γ and γ_0 , defined in Eqs. (96) and (36), respectively, as functions of $\Delta\nu$. The values $\gamma = 1$ and $\gamma_0 = 1$ define the depinning transition point $\Delta\nu_c$ for $v_{imp} = 0.0005e^4/l_B^2$ and $\Delta\nu_c^{(0)}$ in the pure limit, respectively.

$\Delta\nu$	e_x	β_x	α_y	β_y	s_{y1}	s_{y2}	s_{x1}	s_{x2}
0.46	-0.0037	2.26	0.68	2.2	2.2e-6	0.165	0.161	0.076
0.463	-0.0037	1.96	0.34	2.6	2.6e-6	0.143	0.192	0.016
0.466	-0.0037	1.98	0.18	2.9	2.9e-6	0.146	0.215	0.0049
0.47	-0.0035	1.97	0.10	3.4	3.1e-6	0.147	0.252	0.0014
0.48	-0.0034	1.85	0.02	5.0	4.4e-6	0.141	0.382	4e-5

TABLE I: Table of the coefficients of the leading order terms of the self energy and conductivities in the PRSB state at various filling.

C. Constraint for e_x and numerical result for the conductivities

To obtain quantitative results for the conductivities in the PRSB state, we need to numerically solve the SPEs (Eqs. 67) together with the constraint for e_x . This constraint can be obtained, under the assumption of the existence of linear- ω term in $\tilde{\zeta}_x^{\text{ret}}(\omega)$ at small ω , from the first constraint Eq. (79) in the pinned state by examining the limit $e_y \rightarrow 0$. It is easy to find that $g_{xx} \sim \text{const.}$, $g_{xy} \sim |e_y|^{1/2}$, and $g_{yy} \sim |e_y|^{3/2}$. On the other hand, $e^{-W(\pm K_{x0}, 0)}$ tends to a non-vanishing constant as $e_y \rightarrow 0$, while both $e^{-W(0, \pm K_{y0})}$ and $e^{-W(\pm K_{x0}, \pm K_{y0})}$ scale as $|e_y|^{-(\gamma+2)/2}$, where γ was defined in Eq. (96). Plugging these into Eq. (80) yields $U_{xx} \sim \text{const.}$, $U_{xy} \sim |e_y|^{-1/2}$, $U_{yx} \sim |e_y|^{(\gamma+1)/2}$, and

$$U_{yy} \sim |e_y|^{(\gamma-1)/2}. \quad (99)$$

Eq. (79) thus becomes

$$(U_{xx} - 1) \left(c_0 |e_y|^{(\gamma-1)/2} - 1 \right) \sim |e_y|^{\gamma/2}, \quad (100)$$

where c_0 is a constant whose precise value is irrelevant for our discussion. In the PRSB state, $\gamma > 1$ and $e_y = 0$, so that the constraint becomes

$$U_{xx} - 1 = 0. \quad (101)$$

In Appendix D, we discuss another way of satisfying Eq. (100) which leads to an unphysical solution.

We have carried out numerical calculations of the exponents and conductivities for the fillings $\Delta\nu = 0.46, 0.463, 0.466, 0.47, 0.48$, all of which are in the PRSB state. Results for γ are shown as squares in Fig. 7. Clearly, γ increases monotonically with filling factor. Notice that γ at $\Delta\nu = 0.46$ is very close to the critical value 1, and by an extrapolation we conclude that $\Delta\nu_c \simeq 0.459$. By comparing with Fig.3 in the RSB state, we find that $\Delta\nu_c$ agrees with that from the RSB state, yielding a non-trivial check on our numerics. In Fig. 7 we also plot γ_0 (circles) which is computed from Eq. (36) in the pure limit. The critical γ_0 results in a critical filling at the vanishing disorder limit $\Delta\nu_c^{(0)} \simeq 0.432$. The result of $\Delta\nu_c > \Delta\nu_c^{(0)}$ reflects the fact that a stronger disorder strength makes pinning more likely and so increases $\Delta\nu_c$. As we mentioned before, the disorder level we choose is most likely larger than the experimental situation. We expect that in the experimental parameter regime the critical filling for the quantum depinning transition for $N = 3$ is some value between 0.432 and 0.459.

The numerically computed values of $\gamma_{\zeta y}$, $\gamma_{\sigma x}$ and $\gamma_{\sigma y}$ are shown as circles in Fig. (6). We find $\Delta\nu'_c \simeq 0.467$.

Our numerical result also confirms the low-energy behavior of the self-energy Eqs. (77-78) and (89-90). In Tab. 1, we present the coefficients of the leading terms of the self energy. It is clear that e_x is nearly a constant, and β_x and β_y are also moderate functions of $\Delta\nu$. But α_y increases drastically as $\Delta\nu$ approaches $\Delta\nu_c$ from above. We will comment on this in Sec. VII.

It is important to note that the coefficients we find for s_{y1} are numerically very small (see Table I), so that the anomalous divergence near $\omega = 0$ can only be visible at very small frequencies. This suggests that the divergence may be in practice difficult to observe, and indeed it is beyond the numerical accuracy of our calculations too because the frequency grid required would be much finer than can practically be achieved. For frequencies of order $\omega > 10^{-5}$ we find that the anomalous divergence cannot be seen (for the parameters of our calculation) and the finite frequency response appears to be that of an incoherent metal. Interestingly we find that the incoherent contribution to the dynamical conductivity becomes sharply peaked for $\omega < .001$, but this levels off to a constant when the frequency becomes small enough.

Numerical results for the conductivities perpendicular to the stripes at various fillings are shown for a fairly large frequency range in Fig. 8. The low-energy pinning mode is absent, and there is instead a broad peak at high frequencies. We would like to remark that the result at such high energy scales should be taken with a grain of salt,

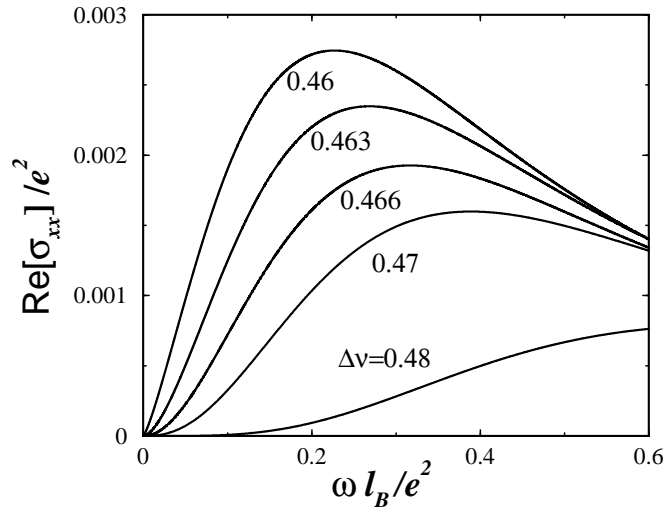


FIG. 8: Real part of conductivity perpendicular to the stripes as a function of frequency in the depinned (PRSB) state. The value $v_{\text{imp}} = 0.0005e^4/l_B^2$ is used. Curves from left to right correspond to $\Delta\nu = 0.46, 0.463, 0.466, 0.47$ and 0.48 respectively. Note that the low-energy pinning mode is absent in the PRSB.

as our elastic model only reproduces the excitation spectrum of the quantum Hall stripes for low energies. The peak may be interpreted as being due to a maximum in the phonon density of states that occurs in the elastic model, and is *not* a pinning peak. For much lower frequencies where our computation is accurate, $\text{Re}[\sigma_{xx}(\omega)]$ shows the power law behavior as expected. For $\Delta\nu = 0.47$ and 0.48 which are larger than $\Delta\nu'_c$, the anticipated $\text{Re}[\sigma_{xx}(\omega)] \simeq \omega^2$ is not visible within our numerical accuracy. As shown in Table I, the coefficient of the ω^2 term, S_{x2} , is much smaller than that of the ω^γ term, S_{x1} , for $\Delta\nu = 0.47$ and 0.48 , again requiring a very fine ω grid to observe. Thus in practice one may observe the anomalous power law dependence over a relatively large range of filling factors.

VII. QUANTUM DEPINNING TRANSITION - KT UNIVERSALITY CLASS

In the previous section, we observed jumps in the low-frequency exponents of $\tilde{\zeta}_y^{\text{ret}}$, $\text{Re}[\sigma_{xx}(\omega)]$ and $\text{Re}[\sigma_{yy}(\omega)]$ at the quantum depinning transition point. In this section, we discuss the connection of these jumps with the universal jump in the superfluid stiffness and the critical exponent of correlation functions of the KT transition²⁶.

The depinning transition we have found is of the KT form, as is clear from the perturbative RG analysis¹⁷. Inserting the smectic form of $D_{yy}(\mathbf{q})$ in Eq. (24) into the action (40) one can see that $d_{yy}(q_x)$ acts as an effective stiffness along the stripes direction. The action in Eqs. (39)-(41) for the stripes phase then can be viewed as a generalized quantum sine-Gordon model: for $v_{\text{imp}} = 0$, the action behaves as a collection of 1+1 dimensional elastic systems, one for each q_x ; the impurity term couples these systems. As is well-known, the two-dimensional classical sine-Gordon model supports a roughening transition³³, which formally is closely related to a smectic-to-crystal transition, and is a dual description of the KT vortex unbinding transition³³.

An interesting aspect of our system is that, in the pure limit, there is no term that is quadratic in ω in either diagonal component of the Green's function, so that there is no analogue of $d_{yy}(q_x)$ in the time direction. However, such a term *is* generated in the self-energy as a result of the variational method when the disorder is present, even in the depinned state. Writing $\text{Re}[\tilde{\zeta}_y^{\text{ret}}(\omega)] \simeq \alpha_y \omega^2$ for small ω , we plot α_y as a function of partial filling factor $\Delta\nu$ above the transition in Fig. 9. One can see the sharp increase as the transition is approached. Such an increase is consistent with the usual RG for the roughening transition, for which the stiffness increases in the RG flows, although one needs to go to higher order in perturbation theory than was undertaken in Ref. 17 to see this. We note finally that α_y *cannot* increase indefinitely: as it increases, the value of γ (Eq. (96)) decreases, eventually crossing the critical value and forcing the system into the fully pinned state. In this state, $\text{Re}[\tilde{\zeta}_y^{\text{ret}}(\omega)] \simeq \alpha_y \omega^2$ no longer vanishes as $q_y, \omega \rightarrow 0$, but rather goes to a constant. This can be roughly interpreted as a system with an infinite stiffness, so that one may associate the transition with a jump in α_y from its critical value to infinity.

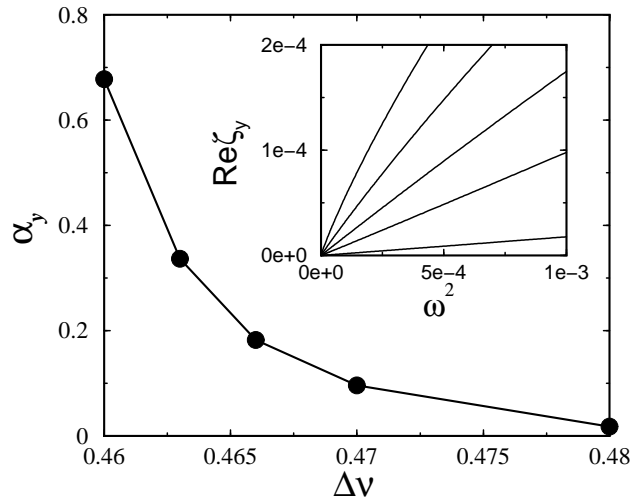


FIG. 9: Coefficient of the quadratic in frequency term in $\text{Re}[\zeta_y^{(\text{ret})}]$ as a function of the partial filling in the depinned (PRSB) state. Inset: $\text{Re}[\zeta_y^{(\text{ret})}]$ as a function of ω^2 . Curves from top to bottom correspond to $\Delta\nu = 0.46, 0.463, 0.466, 0.47, 0.48$, respectively.

VIII. CONCLUSION

In this paper, we have used replicas and the Gaussian variational method to calculate the finite-frequency conductivity of QH stripes in order to see its detailed behavior in the vicinity of the quantum depinning transition. The low-energy degrees of freedom of the QH stripes are described within an effective elastic model that is characterized by a dynamical matrix which is determined by matching to microscopic TDHFA calculation. Our results show that in the pinned state for $\Delta\nu < \Delta\nu_c$, the system is in an RSB state, and the conductivities have resonant peaks for excitation both parallel and perpendicular to the stripes. As $\Delta\nu$ approaches $\Delta\nu_c$ from below, a Debye-Waller factor $W(K_x; K_y \neq 0)$ increases and eventually diverges at $\Delta\nu = \Delta\nu_c$, resulting in a vanishing pinning energy e_y for motion along the stripes. For $\Delta\nu > \Delta\nu_c$, the system enters a new state with *partial* replica symmetry breaking (PRSB), in which the solution has RSB perpendicular to the stripes, but is replica symmetric along them. In this state $\text{Re}[\sigma_{yy}(\omega)]$ has a superconducting response at zero frequency and an anomalous power law behavior for both $\text{Re}[\sigma_{xx}(\omega)]$ and $\text{Re}[\sigma_{yy}(\omega)]$ for $\Delta\nu$ just above the critical value. Moreover, there are jumps in the low-frequency exponents of both the self-energy and conductivities at the transition point, as one might expect for a KT transition.

We conclude by discussing a prominent discrepancy between our results and those of existing experiments. In DC transport, one observes metallic behavior with finite anisotropy rather than the infinite one found in the PRSB state. We believe the missing ingredients from our model are processes allowing hopping of electrons between stripes. These processes are very difficult to incorporate into an elastic model. It is clear that, if relevant in the RG sense, such processes can broaden the δ -function response to yield anisotropic metallic behavior. Our results should apply at frequency scales above this broadening. Indeed, microwave absorption experiments become quite challenging at low frequencies, and it is unclear whether existing measurements of the dynamical conductivity can access the low frequency conductivity in the unpinned state, whether or not it is broadened. In any case, it is interesting to speculate that a true δ -function response might be accessible in structured environments where barriers between stripes may suppress electron hopping among stripes³⁷, or that there may be analogous states for layered 2+1 dimensional classical systems of long string-like objects, which has been shown¹¹ to be closely related to the two-dimensional quantum stripe problem.

Acknowledgments

The authors are especially grateful to R. Lewis, L. Engel, and Y. Chen for many stimulating discussions about this problem, and for showing us their experimental data prior to publication. We are also indebted to T. Giamarchi, G. Murthy, E. Orignac, E. Poisson, and A.H. MacDonald for useful discussions and suggestions. This work was supported by a NSF Grant No. DMR-0414290, by a grant from the Fonds Québécois de la recherche sur la nature et les technologies and a grant from the Natural Sciences and Engineering Research Council of Canada, and by a grant

from SKORE-A program.

APPENDIX A: SUMMARY OF HF AND TDHF FORMALISMS

In a previous work⁷, two of us have shown that, in the HFA, the smectic state (as in the edge state model⁸) is unstable with respect to density modulations along the direction of the stripes. The ground state of the two-dimensional electron gas near half filling of the higher Landau levels is instead an anisotropic two-dimensional Wigner crystal with basis vectors $\mathbf{R}_1 = (0, a_y)$ and $\mathbf{R}_2 = (a_x, a_y/2)$. (One can also see this crystal as an array of 1D Wigner crystals with out-of-phase modulations on adjacent 1D crystals). The electronic density of this crystal is fully determined by the Fourier components of the electronic density $\{\langle n(\mathbf{K}) \rangle\}$ where \mathbf{K} is a reciprocal lattice vector of the oblique lattice shown in Fig. 1.

In our analysis, the Hilbert space is restricted to that of the partially filled Landau level. It is then convenient to define a density of orbit centers or “guiding-center density” $\langle \rho(\mathbf{K}) \rangle$ which is related to the electronic density by the equation

$$\langle n(\mathbf{K}) \rangle = N_\phi F_N(\mathbf{K}) \langle \rho(\mathbf{K}) \rangle, \quad (\text{A1})$$

where N_ϕ is the Landau-level degeneracy and

$$F_N(\mathbf{K}) = e^{-K^2 l_B^2/4} L_N^0 \left(\frac{K^2 l_B^2}{2} \right), \quad (\text{A2})$$

($L_N^0(x)$ is a generalized Laguerre polynomial) is a form factor for an electron in Landau level N . The $\langle \rho(\mathbf{K}) \rangle$'s can be computed⁷ by solving the HF equation of motion for the single particle Green's function

$$\mathcal{G}(\mathbf{K}, \tau) = -\frac{1}{N_\phi} \sum_{X, X'} e^{-\frac{i}{2} K_x (X+X')} \delta_{X, X' - K_y l_B^2} \left\langle \mathcal{T}_\tau c_X(\tau) c_{X'}^\dagger(0) \right\rangle, \quad (\text{A3})$$

with

$$\langle \rho(\mathbf{K}) \rangle = \mathcal{G}(\mathbf{K}, \tau = 0^-). \quad (\text{A4})$$

In Eq. (A3), c_X (c_X^\dagger) is the destruction(creation) operator for an electron in Landau level N with guiding-center X in the Landau gauge.

From the set of $\langle \rho(\mathbf{K}) \rangle$'s computed in the HFA, one can derive the dynamical “density-density” correlation function

$$\chi_{\mathbf{K}, \mathbf{K}'}^{(\rho, \rho)}(\mathbf{q}, \tau) = -N_\phi \langle \mathcal{T}_\tau \tilde{\rho}(\mathbf{q} + \mathbf{K}, \tau) \tilde{\rho}(-\mathbf{q} - \mathbf{K}', 0) \rangle, \quad (\text{A5})$$

in the TDHFA⁷. In Eq. (A5), \mathbf{q} is a vector restricted to the first Brillouin zone of the stripe crystal and $\tilde{\rho} \equiv \rho - \langle \rho \rangle$. By following the poles of $\chi^{(\rho, \rho)}$ with non-vanishing weight as the wavevector \mathbf{q} is varied in the Brillouin zone of the reciprocal lattice, we get the dispersion relation of the phonon and higher-energy collective modes of the stripe state. The equation of motion for $\chi_{\mathbf{K}, \mathbf{K}'}^{(\rho, \rho)}(\mathbf{q}, \tau)$, in the TDHFA, is given by

$$\sum_{\mathbf{K}''} [i\omega_n \delta_{\mathbf{K}, \mathbf{K}'} - M_{\mathbf{K}, \mathbf{K}''}(\mathbf{q})] \chi_{\mathbf{K}'', \mathbf{K}'}^{(\rho, \rho)}(\mathbf{q}, i\omega_n) = B_{\mathbf{K}, \mathbf{K}'}(\mathbf{q}), \quad (\text{A6})$$

where ω_n is a Matsubara bosonic frequency and the matrices $M_{\mathbf{K}, \mathbf{K}'}$ and $B_{\mathbf{K}, \mathbf{K}'}$ are defined by

$$M_{\mathbf{K}, \mathbf{K}'}(\mathbf{q}) = -2i \left(\frac{e^2}{\kappa l_B} \right) \langle \rho(\mathbf{K} - \mathbf{K}') \rangle \times \sin \left[\frac{(\mathbf{q} + \mathbf{K}) \times (\mathbf{q} + \mathbf{K}') l_B^2}{2} \right] [H_N(\mathbf{K} - \mathbf{K}') - X_N(\mathbf{K} - \mathbf{K}') - H_N(\mathbf{q} + \mathbf{K}') + X_N(\mathbf{q} + \mathbf{K}')] \quad (\text{A7})$$

and

$$B_{\mathbf{K}, \mathbf{K}'}(\mathbf{q}) = 2i \sin \left[\frac{(\mathbf{q} + \mathbf{K}) \times (\mathbf{q} + \mathbf{K}') l_B^2}{2} \right] \langle \rho(\mathbf{K} - \mathbf{K}') \rangle \quad (\text{A8})$$

respectively. (Here $\mathbf{a} \times \mathbf{b}$ stands for $a_x b_y - a_y b_x$.)

In Eq. (A7), $H_N(\mathbf{q})$ and $X_N(\mathbf{q})$ are the HF interactions in Landau level N :

$$H_N(\mathbf{q}) = \left(\frac{e^2}{\kappa l_B} \right) \frac{1}{q l_B} e^{-\frac{q^2 l_B^2}{2}} \left[L_N^0 \left(\frac{q^2 l_B^2}{2} \right) \right]^2, \quad (\text{A9})$$

$$X_N(\mathbf{q}) = \left(\frac{e^2}{\kappa l_B} \right) \sqrt{2} \int_0^\infty dx e^{-x^2} [L_N^0(x^2)]^2 J_0(\sqrt{2} x q l_B). \quad (\text{A10})$$

To solve for $\chi_{\mathbf{K}, \mathbf{K}'}^{(\rho, \rho)}(\mathbf{q}, i\omega_n)$, we diagonalize the matrix $M_{\mathbf{K}, \mathbf{K}'}(\mathbf{q})$ by the transformation

$$M = C E C^{-1}, \quad (\text{A11})$$

where C is the matrix of the eigenvectors of M and $E_{i,j} = \varepsilon_j \delta_{i,j}$ is the diagonal matrix of its eigenvalues. The analytic continuation of $\chi_{\mathbf{K}, \mathbf{K}'}^{(\rho, \rho)}(\mathbf{q}, i\omega_n)$ is given by

$$\chi_{\mathbf{K}, \mathbf{K}'}^{(\rho, \rho)}(\mathbf{q}, \omega) = \sum_{j,k} \frac{C_{\mathbf{K}, j}(\mathbf{q}) [C(\mathbf{q})^{-1}]_{j,k} B_{k, \mathbf{K}'}(\mathbf{q})}{\omega + i\delta - \varepsilon_j(\mathbf{q})} \quad (\text{A12})$$

$$\equiv \sum_i \frac{W_i(\mathbf{q} + \mathbf{K}, \mathbf{q} + \mathbf{K}')}{\omega + i\delta - \varepsilon_i}, \quad (\text{A13})$$

where $W_i(\mathbf{q} + \mathbf{K}, \mathbf{q} + \mathbf{K}')$ is the weight of the pole ε_i in the response function. The true density response function is simply

$$\chi_{\mathbf{K}, \mathbf{K}'}^{(n, n)}(\mathbf{q}, \omega) = N_\phi \sum_i \frac{F_N(\mathbf{q} + \mathbf{K}) W_i(\mathbf{q} + \mathbf{K}, \mathbf{q} + \mathbf{K}') F_N(\mathbf{q} + \mathbf{K}')}{\omega + i\delta - \varepsilon_i}. \quad (\text{A14})$$

APPENDIX B: INVERSION RULES FOR MATRICES

The inversion rules for hierarchical matrices in the $n \rightarrow 0$ limit for the case where the entries are scalars may be found in Ref.²⁰. In this appendix we generalize these inversion rules for the situation when the entries are themselves $n_0 \times n_0$ matrices, with our problem corresponding to $n_0 = 2$.

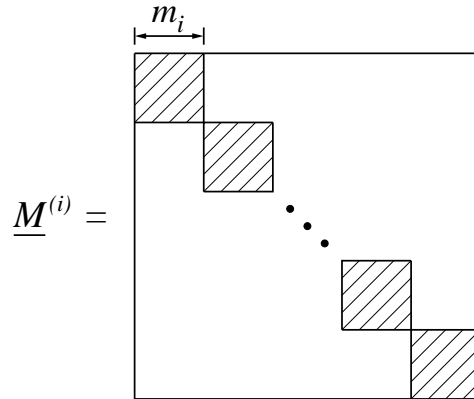


FIG. 10: Schematic structure of the matrix $\underline{M}^{(i)}$. All the matrix elements in the shaded area are 1 and 0 elsewhere.

In the replica method, we introduce n replicas of the system and thus deal with $(n_0 n) \times (n_0 n)$ matrices. In the RSB states, in order to invert matrices in the limit of $n \rightarrow 0$ analytically, we follow the scalar case to assume that the $(n_0 n) \times (n_0 n)$ matrices have a hierarchical structure. This may be described by a set of integers $m_0 (= n), m_1, \dots, m_k, m_{k+1} (= 1)$ where m_i/m_{i+1} is also an integer. Such matrices may be constructed by introducing $k+2$ “block” matrices $\underline{M}^{(i)}$ ($i = 0, \dots, k+1$) all of size $n \times n$. These are defined such that their elements are 1 within the

m_i blocks along the diagonal and 0 elsewhere. These matrices can be used as a basis for a group, so that any $n_0 n$ by $n_0 n$ hierarchical matrix $\underline{\underline{A}}$ can be expressed as

$$\underline{\underline{A}} = \tilde{\hat{a}} \otimes \underline{\underline{1}} + \sum_{i=0}^k \hat{a}_i \otimes [\underline{\underline{M}}^{(i)} - \underline{\underline{M}}^{(i+1)}]. \quad (\text{B1})$$

where $\tilde{\hat{a}}$ and \hat{a}_i are $n_0 \times n_0$ matrices. It is easy to check that

$$(\hat{a}_i \otimes \underline{\underline{M}}^{(j)}) \cdot (\hat{a}_l \otimes \underline{\underline{M}}^{(s)}) = (\hat{a}_i \cdot \hat{a}_l) \otimes (\underline{\underline{M}}^{(j)} \cdot \underline{\underline{M}}^{(s)}). \quad (\text{B2})$$

This means that $\underline{\underline{A}}$ is characterized by $k + 2$ n_0 by n_0 matrices $\tilde{\hat{a}}$ and \hat{a}_i ($i = 0, \dots, k$). In fact, $\underline{\underline{A}}$ is completely parametrized by its topmost row

$$\tilde{\hat{a}} \quad \underbrace{\hat{a}_k \cdots \hat{a}_k}_{m_k} \quad \underbrace{\hat{a}_{k-1} \cdots \hat{a}_{k-1}}_{m_{k-1}} \quad \cdots \cdots \quad \underbrace{\hat{a}_0 \cdots \hat{a}_0}_{m_0}. \quad (\text{B3})$$

We can then define

$$\hat{a}(u) = \begin{cases} \hat{a}_0 & \text{for } n - m_1 < u < n \\ \vdots & \\ \hat{a}_k & \text{for } 1 < u < m_k \end{cases} \quad (\text{B4})$$

to parameterize the off-diagonal element matrices.

We assume that the matrix $\underline{\underline{A}}$ has an inverse matrix $\underline{\underline{B}}$ which because of the group properties should also be a hierarchical matrix, and thus is characterized by $\tilde{\hat{b}}$ and \hat{b}_i ($i = 1, \dots, k$). If we multiply two matrices $\underline{\underline{A}}$ and $\underline{\underline{B}}$ and call the product $\underline{\underline{C}}$, it may be written as

$$\underline{\underline{C}} = \underline{\underline{A}} \cdot \underline{\underline{B}} = \tilde{\hat{c}} \otimes \underline{\underline{1}} + \sum_{i=0}^k \hat{c}_i \otimes [\underline{\underline{M}}^{(i)} - \underline{\underline{M}}^{(i+1)}], \quad (\text{B5})$$

with

$$\tilde{\hat{c}} = \tilde{\hat{a}} \cdot \tilde{\hat{b}} - \sum_{i=0}^k (m_{i+1} - m_i) \hat{a}_i \cdot \hat{b}_i, \quad (\text{B6})$$

$$\hat{c}_i = \hat{a}_i \cdot \tilde{\hat{b}} - m_i \hat{a}_i \cdot \hat{b}_i + \sum_{j=i+1}^k (m_j - m_{j+1}) (\hat{a}_i \cdot \hat{b}_j + \hat{a}_j \cdot \hat{b}_i) - \sum_{j=0}^i (m_{j+1} - m_j) \hat{a}_j \cdot \hat{b}_j. \quad (\text{B7})$$

Now we are in the position to analytically continue the hierarchical matrix to $n \rightarrow 0$. We first analytically continue $\hat{a}(u)$ to be defined for $u \in [1, n]$ and then take the limit $n \rightarrow 0$. The limit $n \rightarrow 0$ then suggests that the hierarchical matrix $\underline{\underline{A}}$ is specified by a diagonal-element matrix $\tilde{\hat{a}}$ and a matrix function $\hat{a}(u)$ for $u \in [0, 1]$. The matrix $\underline{\underline{B}}$ can be analytically continued in the same way. Eqs. (B6-B7) therefore become

$$\tilde{\hat{c}} = \tilde{\hat{a}} \cdot \tilde{\hat{b}} - \int_0^1 du \hat{a}(u) \cdot \hat{b}(u), \quad (\text{B8})$$

$$\hat{c}(u) = (\tilde{\hat{a}} - \langle \hat{a} \rangle) \cdot \hat{b}(u) + \hat{a}(u) \cdot (\tilde{\hat{b}} - \langle \hat{b} \rangle) - \int_0^u dv [\hat{a}(u) - \hat{a}(v)] \cdot [\hat{b}(u) - \hat{b}(v)], \quad (\text{B9})$$

where $\langle \hat{a} \rangle = \int_0^1 dv \hat{a}(v)$. Since $\underline{\underline{B}}$ is the inverse matrix of $\underline{\underline{A}}$, we require

$$\tilde{\hat{c}} = \hat{1}, \quad \hat{c}(u) = \hat{0}. \quad (\text{B10})$$

Differentiating Eq. (B9) with respect to u and using Eq. (B10) leads to

$$\left\{ \tilde{\hat{a}} - \langle \hat{a} \rangle - [\hat{a}](u) \right\} \cdot \hat{b}'(u) + \hat{a}'(u) \cdot \left\{ \tilde{\hat{b}} - \langle \hat{b} \rangle - [\hat{b}](u) \right\} = \hat{0}, \quad (\text{B11})$$

where $[\hat{a}](u) = \int_0^u dv [\hat{a}(u) - \hat{a}(v)]$, and $\hat{a}'(u) = d\hat{a}(u)/du$. By making use of $([\hat{a}](u))' = u\hat{a}'(u)$, Eq. (B11) becomes

$$\left\{ \tilde{\hat{a}} - \langle \hat{a} \rangle - [\hat{a}](u) \right\} \cdot \left\{ \tilde{\hat{b}} - \langle \hat{b} \rangle - [\hat{b}](u) \right\} = \text{const.} \quad (\text{B12})$$

To determine the constant matrix in Eq. (B12), we examine Eqs. (B8) and (B9) at $u = 1$ and get

$$\left[\tilde{\hat{a}} - \hat{a}(1) \right] \cdot \left[\tilde{\hat{b}} - \hat{b}(1) \right] = \hat{1}. \quad (\text{B13})$$

So $\text{const.} = \hat{1}$, and Eq. (B12) gives

$$\left\{ \tilde{\hat{b}} - \langle \hat{b} \rangle - [\hat{b}](u) \right\} = \left\{ \tilde{\hat{a}} - \langle \hat{a} \rangle - [\hat{a}](u) \right\}^{-1}, \quad (\text{B14})$$

which can be inserted into Eq. (B11) to produce one of the inversion rules

$$\hat{b}(u) - \hat{b}(v) = \int_u^v dy \left\{ \tilde{\hat{a}} - \langle \hat{a} \rangle - [\hat{a}](y) \right\}^{-1} \cdot \hat{a}'(y) \cdot \left\{ \tilde{\hat{a}} - \langle \hat{a} \rangle - [\hat{a}](y) \right\}^{-1}. \quad (\text{B15})$$

This is very similar to Eq. (AII.5) in Ref. 20. Eqs. (B15) and (B13) lead to

$$\tilde{\hat{b}} - \hat{b}(u) = \left[\tilde{\hat{a}} - \hat{a}(1) \right]^{-1} - \int_u^1 dv \left\{ \tilde{\hat{a}} - \langle \hat{a} \rangle - [\hat{a}](v) \right\}^{-1} \cdot \hat{a}'(v) \cdot \left\{ \tilde{\hat{a}} - \langle \hat{a} \rangle - [\hat{a}](v) \right\}^{-1}. \quad (\text{B16})$$

This is the inversion rule we have used in our work [see Eq. (63) in the text].

For completeness, we also show, without giving the details of the derivation, some other inversion rules as well as the formula for $\lim_{n \rightarrow 0} \left(\frac{1}{n} \text{Tr} \ln \underline{\underline{A}} \right)$ which appears in the expression of free energy:

$$\tilde{\hat{b}} = \left(\tilde{\hat{a}} - \langle \hat{a} \rangle \right)^{-1} \cdot \left\{ \hat{1} - \int_0^1 \frac{du}{u^2} [\hat{a}](u) \cdot \left(\tilde{\hat{a}} - \langle \hat{a} \rangle - [\hat{a}](u) \right)^{-1} - \hat{a}(0) \cdot \left(\tilde{\hat{a}} - \langle \hat{a} \rangle \right)^{-1} \right\}, \quad (\text{B17})$$

$$\hat{b}(u) = - \left(\tilde{\hat{a}} - \langle \hat{a} \rangle \right)^{-1} \cdot \left\{ \hat{a}(0) \cdot \left(\tilde{\hat{a}} - \langle \hat{a} \rangle \right)^{-1} + \frac{1}{u} [\hat{a}](u) \cdot \left(\tilde{\hat{a}} - \langle \hat{a} \rangle - [\hat{a}](u) \right)^{-1} \right\}$$

$$\lim_{n \rightarrow 0} \left(\frac{1}{n} \text{Tr} \ln \underline{\underline{A}} \right) = \ln \det \left(\tilde{\hat{a}} - \langle \hat{a} \rangle \right) + \text{Tr} \left[\hat{a}(0) \cdot \left(\tilde{\hat{a}} - \langle \hat{a} \rangle \right)^{-1} \right] - \int_0^1 \frac{du}{u^2} \ln \left[\frac{\det \left(\tilde{\hat{a}} - \langle \hat{a} \rangle - [\hat{a}](u) \right)}{\det \left(\tilde{\hat{a}} - \langle \hat{a} \rangle \right)} \right]. \quad (\text{B18})$$

APPENDIX C: SPE'S FOR THE RETARDED SELF ENERGY

In this Appendix, we analytically continue the SPE's (57) for the Matsubara self energy in order to derive the SPE's (67) for the retarded self energy. We rewrite Eq. (57) as

$$\tilde{\zeta}_\alpha(\omega_n) = \int_0^1 du \zeta_\alpha(u) + 4v_{\text{imp}} \int_0^{1/T} d\tau V'_{\alpha\alpha} \left[\tilde{B}(\tau) \right] - 4v_{\text{imp}} J(\omega_n), \quad (\text{C1})$$

where $J(\omega_n)$ is the Fourier transform in Matsubara frequencies of

$$J_0(\tau) = \exp \left[-\frac{1}{2} \sum_\mu K_\mu^2 \tilde{B}_{\mu\mu}(\tau) \right] \quad (\text{C2})$$

with $\tilde{B}_{\mu\mu}(\tau)$ being defined in Eq. (59). Obviously, $J_0(\tau)$ is a Matsubara correlation function, and its corresponding real-time ordered correlation function reads

$$\tilde{J}_0(t) = iJ_0(\tau \rightarrow it) = \theta(t)J_1(t) + \theta(-t)J_2(t), \quad (\text{C3})$$

where $J_1(t) = \tilde{J}_0(t > 0)$, $J_2(t) = \tilde{J}_0(t < 0)$ with the relation $J_2(-t)/i = (J_2(t)/i)^*$, and $\theta(t)$ is the step function. The retarded function becomes

$$J_0^{\text{ret}}(t) = \theta(t)[J_1(t) - J_2(t)]. \quad (\text{C4})$$

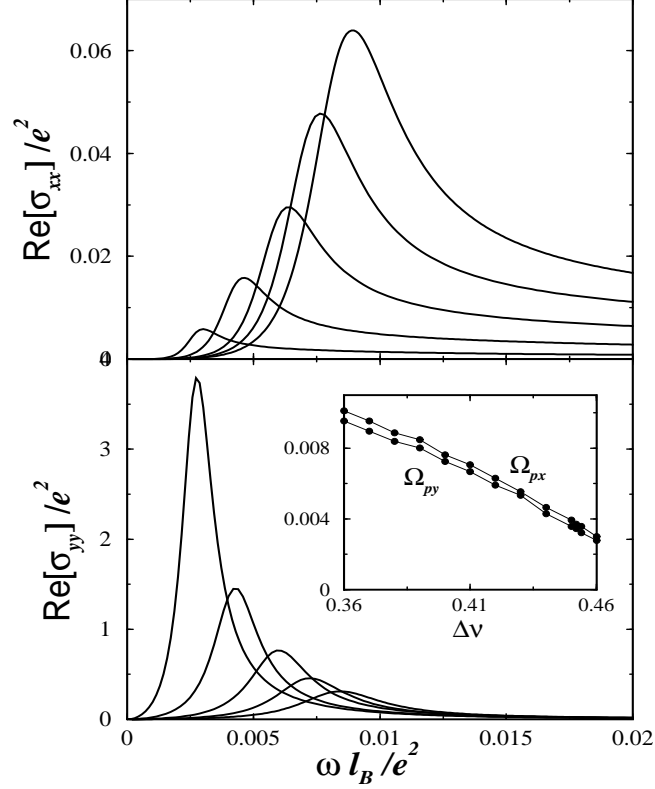


FIG. 11: Real part of conductivity perpendicular to the stripes (a) and parallel to the stripes (b), in the unphysical solution. Curves from right to left correspond to $\Delta\nu = 0.46, 0.44, 0.42, 0.4, 0.38$, respectively. Smaller disorder strength $v_{\text{imp}} = 0.0001e^4/l_B^2$ is used. Inset in (b): Peak frequencies as functions of the partial filling.

Using the Nambu representation

$$\tilde{G}_{\mu\nu}(\mathbf{q}, \omega_n) = -\frac{1}{\pi} \int_{-\infty}^{\infty} df \frac{A_{\mu}(f)}{i\omega_n - f}, \quad (\text{C5})$$

where $A_{\mu}(f)$ is defined in Eq. (69), we find that $\tilde{B}_{\mu\mu}(\tau)$ in Eq. (59) becomes

$$\tilde{B}_{\mu\mu}(\tau) = \frac{1}{\pi} \int_0^{\infty} df A_{\mu}(f) \left[T \sum_{\omega_n} (1 - \cos \omega_n \tau) \frac{2f}{\omega_n^2 + f^2} \right]. \quad (\text{C6})$$

We can then easily sum over the Matsubara frequency in the above equation to get

$$\tilde{B}_{\mu\mu}(\tau) = \frac{1}{\pi} \int_0^{\infty} df A_{\mu}(f) \left[1 - e^{-|\tau|f} + \frac{2[1 - \cosh(f\tau)]}{e^{u/T} - 1} \right]. \quad (\text{C7})$$

Apparently, at $T = 0$, the last term inside the parentheses in Eq. (C7) vanishes. Inserting Eq. (C7) into Eq. (C2) and following the procedure described in Eqs. (C3) and (C4), we find that at $T = 0$,

$$J_0^{\text{ret}}(t) = i\theta(t) \text{Im} \exp \left[-\sum_{\mu} \frac{K_{\mu}^2}{\pi} \int_0^{\infty} df A_{\mu}(f) (1 - e^{-|\tau|f}) \right]. \quad (\text{C8})$$

From Eqs. (C1) and (C8) and noting that $J_0^{\text{ret}}(\omega) = \int_{-\infty}^{\infty} dt e^{i\omega t} J_0^{\text{ret}}(t)$, we immediately obtain Eq. (67).

APPENDIX D: UNPHYSICAL SOLUTION OF THE SPE'S

In our numerical search, we also notice the existence of another solution which we present here and argue is unphysical. Fig. 11 shows the result of the conductivities from this solution which corresponds to a much smaller

disorder level. Both $\text{Re}[\sigma_{xx}(\omega)]$ and $\text{Re}[\sigma_{yy}(\omega)]$ show the pinning behavior and the peak frequencies move in as also shown in the inset of Fig. 11 (b). However, unlike in the solution we presented in the text, no quantum depinning transition occurs.

Interestingly, this solution displays a peak move-in behavior that is reminiscent of what is seen in the physical solution. This is the result of a decreasing e_y , due to the increasing $W(K_x; K_y \neq 0)$ with the partial filling $\Delta\nu$. However, at small e_y , unlike in the other solution, the constraint (100) is not satisfied through $U_{xx} = 1$, but instead through $U_{yy} = 1$. This can be seen from Eq. (99), according to which U_{yy} will rapidly decrease from very large values to very small values right near $\gamma = 1$. This means that near this value U_{yy} must pass through one, satisfying the constraint. In this solution, γ remains very close to one over a range of filling factors, and does so by making $|e_x|$ very large, even for small v_{imp} . This implies an unphysically large pinning for sliding perpendicular to the stripes. Because of this, and the close agreement between the other solution and the perturbative RG results, we ignore this solution to the SPE's as physically unreasonable.

-
- ¹ A. A. Koulakov, M. M. Fogler, and B. I. Shklovskii, Phys. Rev. Lett. **76**, 499 (1996); M. M. Fogler, A. A. Koulakov, and B. I. Shklovskii, Phys. Rev. B **54**, 1853 (1996); R. Moessner and J. T. Chalker, *ibid.* **54**, 5006 (1996).
- ² I. L. Aleiner and L. I. Glazman, Phys. Rev. B **52**, 11296 (1995).
- ³ N. Shibata and D. Yoshioka, Phys. Rev. Lett. **86**, 5755 (2001).
- ⁴ E. H. Rezayi, F. D. M. Haldane, and K. Yang, Phys. Rev. Lett. **83**, 1219 (1999); F. D. M. Haldane, E. H. Rezayi, and K. Yang, *ibid.*, **85**, 5396 (2000).
- ⁵ M. P. Lilly *et al*, Phys. Rev. Lett. **82**, 394 (1999); **83**, 820 (1999); R. R. Du *et al*, Solid State Commun. **109**, 389 (1999); W. Pan *et al*, Phys. Rev. Lett. **83**, 820 (1999); K. B. Cooper *et al*, Phys. Rev. B **60**, 11285 (1999).
- ⁶ E. Fradkin and S. A. Kivelson, Phys. Rev. B **59**, 8065 (1999).
- ⁷ R. Côté and H. A. Fertig, Phys. Rev. B **62**, 1993 (2000).
- ⁸ A.H. MacDonald and M.P. A. Fisher, Phys. Rev. B **61**, 5724 (2000); A. Lopatnikova *et al.*, *ibid.* **64**, 155301 (2001).
- ⁹ For a review, see J. Voit, Rep. Prog. Phys. **58**, 977 (1995).
- ¹⁰ E.B. Kolomeisky and Joseph P. Straley, Rev. Mod. Phys. **68**, 175 (1996).
- ¹¹ H. A. Fertig, Phys. Rev. Lett. **82**, 3693 (1999).
- ¹² H. Fukuyama and P. A. Lee, Phys. Rev. B **17**, 535 (1978).
- ¹³ A. I. Larkin, Sov. Phys. JETP **31**, 784 (1970); A. I. Larkin and Y. N. Ovchinnikov, J. Low. Temp. Phys. **34**, 409 (1979).
- ¹⁴ T. Giamarchi and H.J. Schulz, Phys. Rev. B **37**, 325 (1988); C. Kane and M.P.A. Fisher, Phys. Rev. Lett. **68**, 1220 (1992).
- ¹⁵ R.M. Lewis, P.D. Ye, L.W. Engel, D.C. Tsui, L.N. Pfeiffer, and K.W. West, Phys. Rev. Lett. **89**, 136804 (2002) .
- ¹⁶ R. Lewis, L. Engel and Y. Chen, private communication.
- ¹⁷ Hangmo Yi, H. A. Fertig, and R. Côté, Phys. Rev. Lett. **85**, 4156 (2000). Note in that letter, the stripes are assumed to be along the \hat{x} direction.
- ¹⁸ M.-R. Li, H.A. Fertig, R. Côté, and H. Yi, Phys. Rev. Lett. **92**, 186804 (2004).
- ¹⁹ M. Mézard, G. Parisi, and M. Virasoro, *Spin Glass Theory and Beyond* (World Scientific, Singapore, 1987).
- ²⁰ M. Mézard and G. Parisi, J. Phys. I **1**, 809 (1991).
- ²¹ T. Giamarchi and P. Le Doussal, Phys. Rev. B **53**, 15206 (1996).
- ²² T. Giamarchi and P. Le Doussal, Phys. Rev. B **52**, 1242 (1995). The replica and GVM was applied to vortex lattice system to predict the Bragg glass phase, which was later on supported by Monte Carlo simulations [M. J. P. Gingras and D. A. Huse, Phys. Rev. B **53**, 15193 (1996).].
- ²³ T. Giamarchi and E. Orignac, in *Theoretical Methods for Strongly Correlated Electrons*, CRM Series in Mathematical Physics (Spring, Berlin) (also cond-mat/0005220).
- ²⁴ R. Chitra, T. Giamarchi and P. Le Doussal, Phys. Rev. Lett. **80**, 3827 (1998); Phys. Rev. B **65**, 035312 (2002). These works address the pinned Wigner crystal problem by using the replica and GVM and reveal a quite broad pinning peak. Whereas some other approaches obtain a very narrow pinning peak [H. A. Fertig, Phys. Rev. B **59**, 2120 (1999); M. M. Fogler and D. A. Huse, *ibid.* **62**, 7553 (2000)]. We have found that the latter approach is consistent with the former two in the weak disorder limit. The underlying cause of the narrowing is due to a paucity of low-lying phonon states in the isotropic crystal, which does not occur for the stripe state⁷.
- ²⁵ E. Orignac and R. Chitra, Europhys. Lett. **63**, 440 (2003). Note that in this work, some approximations were used valid only when the system is pinned for motion along the stripes, leading to results quite different than ours.
- ²⁶ D. R. Nelson and J. M. Kosterlitz, Phys. Rev. Lett. **39**, 1201 (1977).
- ²⁷ See article by R. Kubo, S.J. Miyake, and N. Hashitsume, in *Solid State Physics* **17** (Academic Press, New York, 1965).
- ²⁸ M. M. Fogler, in *High Magnetic Fields: Applications in Condensed Matter Physics and Spectroscopy*, ed. by C. Berthier, L.-P. Levy, G. Martinez (Springer-Verlag, Berlin, 2002).
- ²⁹ V. L. Berezinskii, Sov. Phys. JETP **38**, 620 (1974).
- ³⁰ To use discrete fast-Fourier transformation to compute the integrals over ω and t , we have to set a typical stepsize in frequency to be much smaller than e_x and e_y and the pinning peak widths. These quantities are dependent on the disorder level. On the other hand, the frequency stepsize is inversely proportional to the large- t cutoff. As the depinning transition is approached and in the depinned state that we will discuss in the next section, to see all the interesting features at small

ω we need to use very large cutoff. We thus need to compromise on the disorder level in order to capture the interesting physics at low frequencies.

³¹ V. Dotsenko, *Introduction to the Replica Theory of Disordered Statistical Systems*, (Cambridge, New York, 2001).

³² W. Kohn, Phys. Rev. **133**, A171 (1964).

³³ P.M. Chaikin and T.C. Lubensky, *Principles of Condensed Matter Physics* (Cambridge University Press, New York, 1995).

³⁴ We want to mention that the weight of this delta function term is not computed accurately in the current method since this term has to be obtained along with the $\omega_n = 0$ mode of $\tilde{\zeta}$.

³⁵ The anomalous finite frequency response for $\sigma_{yy}(\omega)$ was not noticed in our early analysis of these results, and so was not reported in Ref. 18.

³⁶ See, for example, S. Kragset, A. Sudbo, and F.S. Nogueira, Phys. Rev. Lett. **92**, 186403 (2004).

³⁷ A. Endo and Y. Iye, Phys. Rev. B **66**, 075333 (2002).